School of Chemistry

The effect of CVD diamond growth and subsequent surface termination on the bactericidal activity of black silicon

Olivia Dunseath

This thesis is submitted in partial fulfilment of the requirements for the Honours Degree of MSci (Bsc) at the University of Bristol

Supervisor: Paul May

Second Assessor: Neil Fox

Physical and Theoretical Group

ABSTRACT

Due to every increasing antibiotic resistance, the need for antibacterial surfaces that do not rely on a chemical mechanism is more prevalent than ever, for use in applications such as coatings of biological implants. Mechano-bactericidal surfaces have been established as a promising solution, with nanostructures present on the surface key to causing a non-specific physical mechanism of cell death. Black silicon (bSi), a synthetic example of such a surface, has attracted much research due to the high tuneability of the method of fabrication employed, despite its very brittle nature. Bacteria-resistant surfaces are also of interest, due to their ability to repel bacteria and therefore limit colonisation. These can be fabricated by anchoring of polymers to a surface to alter its wettability.

In this project, investigations into the bactericidal capability of uncoated and diamond coated black silicon were continued by characterisation and testing of bSi needles of average length 4.6 µm. It was demonstrated that the uncoated needles exhibited an average cell death percentage of 58.1%, a performance that was hindered upon diamond coating, but not removed.

Research was expanded into combining bactericidal and bacteria-resistant properties through replacement of hydrogen surface terminations on the diamond film with hydrophilic oxygen and amine containing groups, and hydrophobic fluorine groups, *via* plasma treatment. Alterations to surface wettability were confirmed by changes in surface contact angle. **B**acteria Live/Dead assays were used to elucidate the positive correlation between cell adhesion and wettability. Cell death percentage was found to be independent of wettability, supporting the theory of a completely physical mechanism.

The uncoated black silicon produced the most promising results for both bactericidal and bacteria-resistant properties, with lowest cell adhesion and highest cell death percentage of all materials tested.

ACKNOWLEDGEMENTS

I would like to thank my supervisor Professor Paul May for his ideas, guidance and unwavering support throughout the year, Ed Smith for all his suggestions and assistance, Dr Neil Fox, and the rest of the diamond group.

Thanks go to Tarik Al-Jeda for the time he was able to dedicate to helping progress my work whilst completing his own project.

I would like to thank the Oral and Microbiology group for accommodating me and my experiments at such short notice, particularly Sophie King and Josh Jenkins for all their help in introducing me to an area of scientific knowledge and research that was unfamiliar to me.

CONTENTS

1 INTRODUCTION

1.1 THE FIGHT AGAINST BACTERIAL INFECTION

Microbial infection is one of the greatest challenges still faced in healthcare, with healthcare associated infections (HAIs) accounting for 100 000 deaths in the US in 2002[1]. Spread of bacteria in environments such as hospitals is almost unavoidable, and the most prevalent reason for occurrence of these infections in patients is attributed to implantation of contaminated medical devices[2]. Ranging from catheter insertions to joint replacements to pacemakers, as a result of an ageing population and advances in medicine, implantation operations are becoming increasingly commonplace; it is estimated that everyone alive today will undergo at least one such procedure in their lifetime[3]. Therefore, the area of research into preventing bacterial infection is more essential than ever.

Bacterial infection occurs when bacterial cells encounter a suitable surface on which they are able to adhere, grow and multiply, which can lead to formation of a biofilm. Bacterial biofilms are populations of bacteria cells that attach irreversibly and live in organised structures at an interface[4],forming a microcolony (Figure 1). Once a bacterial colony is established, it becomes much more resilient to antibacterial attack, as the effect of antibiotic treatment is largely limited to the outer layer of the film[5]. Biofilm cells have been shown to be 10–1,000-fold less susceptible to attack from antimicrobial agents than the same bacterium grown in free-floating culture[6]. According to the US National Institutes of Health, biofilms account for over 80% of microbial infections in the body[7], commonly causing diseases such as colitis, conjunctivitis and gingivitis, and have also shown to be able to colonise medical devices[8].

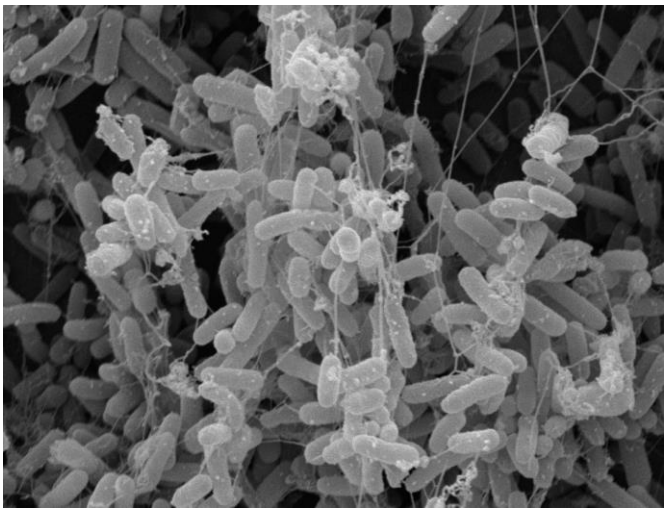

Figure 1 - SEM image showing an example of an E. coli *biofilm* [9]

Antibacterial surfaces are surfaces that reduce the ability of bacteria cells to attach and multiply, hence combatting biofilm formation. The need for such surfaces is obvious – as well as to prevent transfer of infection in medical settings, the coating of materials such as aquatic flow systems and textiles in bacteria can severely affect their function. The fabrication of a viable commercial bactericidal material would have worldwide implications, with the potential to be used to coat everyday household and workplace items such as door handles and keyboards, to inhibit the transmission of bacterial infection.

There are three main types of antibacterial surface; bacteria-resistant, bacteria-release, and bactericidal, which each combat bacteria proliferation in different ways. Two of these classifications will be explored in further detail, informing research into synthesis of new antibacterial surfaces, along with the characteristics that contribute to their properties. To gain better insight into the function of these surfaces, the structure and composition of a typical bacteria cell must be understood.

1.1.1 Bacteria cell structure

Bacteria cells are prokaryotic – without a nucleus – and can be divided into two classes; Gram-positive and Gram-negative. The difference between them arises in the cell wall structure. This wall is what provides the cell with its strength and resilience. In almost all cases, bacteria cells are covered in the compound peptidoglycan (PG), which provides rigidity and surrounds the cell membrane. PG contains repeating units of disaccharides that are cross-linked by pentapeptide side chains. In Gram-positive bacteria, the PG exists as a single layer ranging from 30-100 nm in thickness. However, in Gram-negative strains the wall is more complex, comprising of a PG layer 4-5 times thinner than in Gram-positive, which is followed by the second outer membrane – a lipid bilayer, mainly made-up of lipopolysaccharide[10 11] (Figure 2). The space between the outer and inner membranes within which

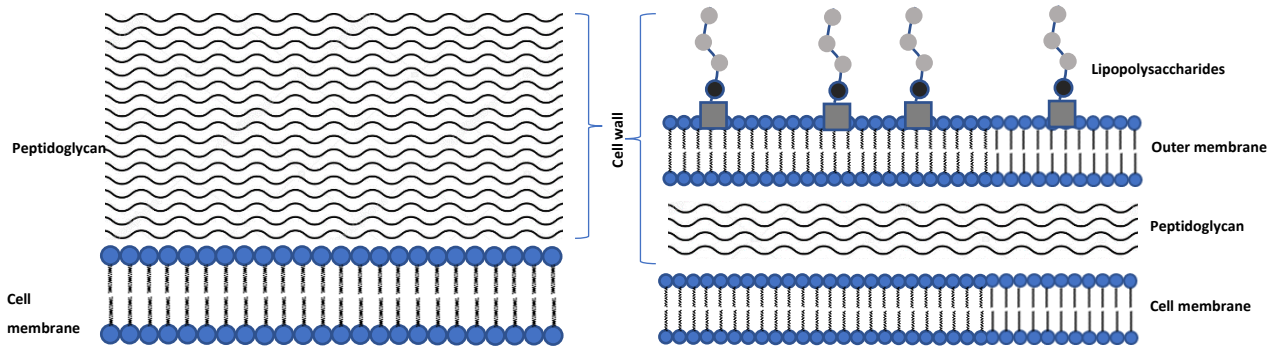

Figure 2 - Diagram displaying the differences in cell wall composition between Gram-positive (left) and Gram-negative (right) bacteria cells.

the PG is situated is an aqueous compartment called the periplasm, similar to but more viscous than cytoplasm.

Gram-negative bacteria also have the capability to express organelles known as fimbriae, or attachment pili, from the cell. These hair-like appendages are made from proteins, and are used to facilitate cell attachment to surfaces. They carry adhesives known as extracellular polymeric substance (EPS), which are used to anchor cells to a surface and withstand shear forces. Expression of fimbriae from a bacterium is a sign that the cell is functioning successfully and is healthy.

1.1.1.1 E. coli

Escherichia coli is a Gram-negative bacterium, commonly found in the digestive system of mammals. Most strains are harmless, and can be grown and cultured easily and inexpensively in a laboratory setting. For this reason it is commonly used in early-stage bactericidal testing. *E. coli* cells use fimbriae as one of their primary mechanisms of virulence; their presence greatly enhancing the bacteria's ability to attach to a surface and cause infection[12].

1.2 Bacteria-Resistant Materials

Bacteria-resistant materials are those which reduce bacterial adhesion to a surface in the first instance. Prevention of bacteria proliferation on a surface is an important property of antibacterial materials, as it greatly reduces the chance of biofilm formation - the most obvious method to prevent biofilm formation on a surface is to stop cells attaching at all. This property can be achieved through application of anti-adhesive coatings onto a surface, the most common form of which are polymeric coatings such as hydrophilic polysaccharides and zwitterionic polymers[13]. Morra *et al* demonstrated the reduction in cellular adhesion onto a surface by coating with aluronic acid and alginic acid, two examples of polysaccharides[14]. The mechanism for this reduction was thought to occur as a result of the increased stability these molecules provide to aqueous suspensions, thus decreasing non-specific interactions between suspended cells and a surface.

1.2.1 Bacteria adhesion

The adhesion of bacteria onto a surface is a complicated process, but basically proceeds in two stages: an initial, rapid, and reversible interaction, followed by a slow, irreversible adhesion through specific and nonspecific interactions[15 16]. As previously discussed, ability of bacteria to adhere to a surface is influenced largely by their 'anchoring' fimbriae, but is also affected by a number of surface properties, most notably wettability and roughness.

1.2.1.1 Surface wettability

Wetting is defined as the ability of a liquid to maintain contact with a surface. When the liquid in question is water, the wettability can also be described as it's hydrophilicity. The hydrophilicity of a surface is thought to play a major role in bacterial adhesion, although depending on the environment, both hydrophilic and hydrophobic surfaces can provide advantages. As previously noted, anchoring of hydrophilic polymer chains onto surfaces has been shown to reduce bacteria cell adhesion. In aqueous medium, hydrophilic surfaces are thought to strongly adsorb a layer of water molecules, which can hinder adhesion of bacteria by providing a barrier, either sterically or energetically[17]. This is useful for applications such as membranes used in desalination or wastewater treatment, which operate in aqueous environments[18].

At the other end of the spectrum, several studies have focused on the relationship between hydrophobicity of a surface and cellular adhesion. Simply, it was found that bacteria cells are less able to 'stick' to hydrophobic and superhydrophobic surfaces, and are hence less likely to proliferate and form a biofilm[19 20]. This property can also provide advantages in aqueous medium, where an air layer can form between cells and surface, thus creating a phase barrier that bacteria would have to cross to accumulate on the surface[21].

The wettability of a surface can be measured by its contact angle, with increasing hydrophobicity causing increasing angle.

1.2.1.2 Surface roughness

Surface roughness is intrinsically linked to surface wettability[22]; it has been observed that surface roughness causes a hydrophobic liquid to behave as if it were more hydrophobic and a hydrophilic liquid to behave as if it were more hydrophilic[23]. This was theorised to be due to rough surfaces extending the solid-liquid interface area in comparison with projected smooth surfaces.

Decuzzi and Ferrari designed a mathematical model to show how cellular adhesion to an inert surface varies as a function of substrate roughness[24]. They identified three regimes as a function of the surface energy of the substrate; for low surface energy, surface roughness decreases cellular adhesion, for intermediate surface energies, roughness does not affect adhesion, and for high surface energy, an optimal roughness can be identified to maximize cellular adhesion.

1.3 BACTERICIDAL MATERIALS

Bactericidal materials are those which deactivate and/or destroy bacteria cells on contact, typically through a chemically-altering mechanism[25]. Historically, these surfaces are fabricated in as simple a way as attaching anti-bacterial compounds such as penicillin or triclosan (TCS)[26] to an existing surface.

However, a major issue with this type of surface is that they are reliant on the activity of an antibacterial agent. Antibiotics are used heavily in the fields of healthcare and agriculture, which has led to resistance becoming more and more widespread[27]. As a result of this, in addition to the fact that biofilms are by nature resistant to antibacterial attack, the focus of research has shifted towards synthesis of bactericidal materials that are able to function via a non-specific physico-mechanism, thus eliminating the need for active agents. Nanostructuring of materials has emerged as a promising route to achieve this physical mechanism, with surfaces coated in nanoscale spikes or protrusions shown to be capable of physically rupturing the cell wall[28], henceforth referred to as mechano-bactericidal. Inspiration for this research has been drawn from natural nanostructured surfaces (NSS).

1.3.1 Naturally occurring mechano-bactericidal surfaces

The first reported example of a natural bactericidal surface was the wings of the cicada (*Psaltoda claripennis*)[29]. Examination of the wing surface showed a regular array of hexagonally packed nanopillars, each 200 nm in length (Figure 3). The wings were shown to be effective at killing *P. aeruginosa* cells, and the mechanism of cell death was established to be purely physical. This was done through significant alteration of the surface chemistry of the wings by Au-coating, making it hydrophilic, with no difference in efficacy observed.

Similar in structure to cicada wings, dragonfly wings (*Orthetrum villosovittatum*) were shown to exhibit the same mechano-bactericidal capabilities against *E. coli*[30]. However, the NSS differed from previously researched surfaces in that the length of pillars was bimodal, with shorter (189 nm) and longer (311 nm) pillars interspersed on the surface.

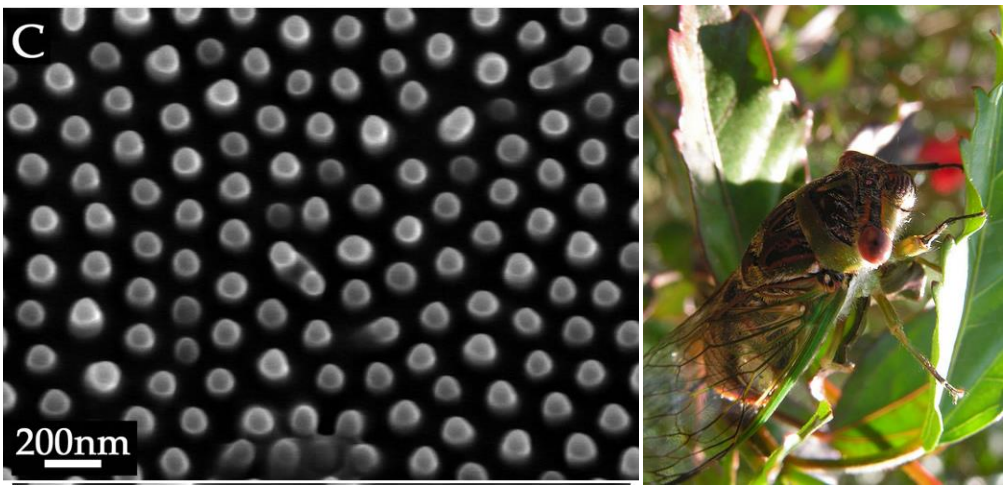

Figure 3 - Top-down view (left) of the nanopillars present on wings of cicadas (right). Taken from [40].

The skin of the *gecko Lucasium steindachneri* was revealed to also exhibit this property[31], with SEM confirming a nanostructure comprising of individual spines of 4 µm long with slight curvature[32].

1.3.2 Physical mechanism of cell death

A number of physical models have been developed to aid in the understanding of the contact killing mechanism exhibited by NSS such as the cicada wing. Each of these make different assumptions of the cell wall and nanoprotrusion.

Pogodin *et al* [33] developed a theory in which the bacteria cell wall was assumed as a thin elastic layer, due to the order of magnitude difference in width between the cicada wing's nanopillars (100 nm) and the cell wall (10 nm). The process of adsorption of the cell onto the nanopillars led to a larger contact surface area as the cell stretches non-uniformly to fill the spaces between pillars. If the degree of stretching was found to be sufficient, it would lead to the rupturing of the cell.

Xue *et al* [34] expanded on this by using the 'stretching' theory. They defined the stretching degree as the difference between the surface areas of the cell that are in contact (S_A) or not in contact (S_B) with the nanopillars (Figure 4). Again, rupturing was said to occur if the stretching degree exceeded a threshold. Through experimentation and modelling, it was concluded that physical interactions between cell and NSS are not the only contributors that lead to cell adhesion and rupture, with other factors, including gravitational forces acting on the cell and van der Waals interactions also playing a role. Additionally, they found that Gram-negative bacteria were more easily destroyed, as their maximum membrane stretching capability was found to be larger than for Gram-positive, indicating that the thinner PG walls were more malleable, and deformation was greater when in contact with the nanopillar coated surface. In other words, Gram-positive strains prove more difficult to kill due to the thicker cell wall allowing extra rigidity. This increased rigidity means the degree of stretching is reduced and hence the threshold is less frequently met.

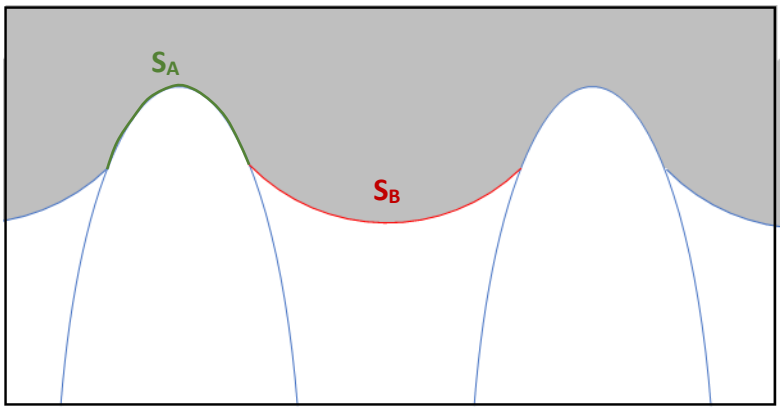

Figure 4 - Side elevation diagram of a bacterial cell sinking onto two nanopillars, where S_A is the surface area of the cell wall in contact with the pillar, and S_B is the surface area suspended between the two pillars.

Li *et al* [35] created a model which was concerned with the total free energy change when a cell is attached to an NSS such as the cicada wing, when compared to a flat surface. The cell was again assumed as a thin elastic layer, but in this instance the stretching degree was defined as the increase in surface area of a cell on contact with a surface compared to its equilibrium surface area: $\Delta S/S_0$. Rupturing was theorised to occur due to the increase in contact adhesion area that is caused by contact with an NSS (Figure 5).

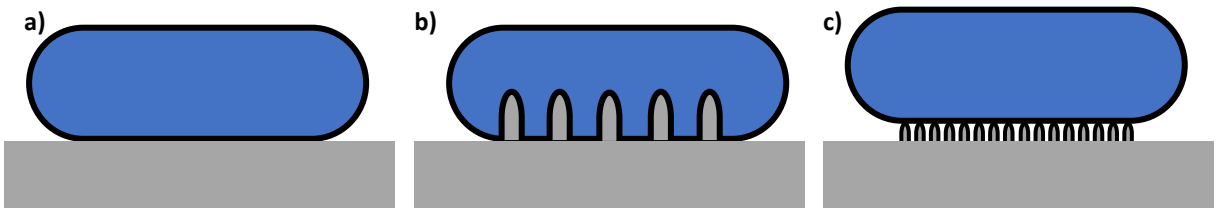

Figure 5 - Diagram showing the settling of a bacteria cell onto a) a flat surface, b) an NSS where the cell can sink down and deform, c) an NSS with more dense spikes where the cell rests on top – the 'bed of nails' effect.

However, for calculation of free energy change this model assumed length of the nanopillars to be several hundred nanometres, leading to the assumption that the bacterial cell can be completely adhered to the nanopillars, as shown in Figure 5b. When considering pillars of longer length, this assumption is unrealistic, as bacteria cells are typically no more than a micron in diameter, and without complete transmission of the pillar through both sides of the cell, this cannot be achieved.

The effect of different nanostructure properties on $\Delta S/S_0$ was modelled, with findings that increasing adhesion energy causes a linear increase in $\Delta S/S_0$, and increasing pillar density causes increased $\Delta S/S_0$ up to a maximum value. This maximum tip density after which no improvement in cell death was expected can be likened to the real-life phenomena known as the 'bed-of-nails' effect[36]. Illustrated in Figure 5c, it shows that when a certain tip density is passed, the space between protrusions is insufficient to allow deformation of the membrane – it has too many points of contact and is therefore able to rest on the surface as if it were flat.

Taking a different approach, Bandara *et al* [30] hypothesised that bacteria cell death on an NSS was initiated by a combination of strong adhesion between nanopillars and bacterium EPS layer, as well as shear force when immobilized bacterium attempts to move on the NSS. The observation of Diu *et al*[37] corroborated this theory. Assessing three motile bacteria (*P. aeruginosa, E. coli,* and *B. subtilis*) and three low- or non-motile species (*S. aureus, Enterococcus faecalis,* and *Klebsiella pneumonia*) on a titanium substrate covered with titania nanowires, they observed that significant bactericidal activities occurred for motile bacteria, but little or negligible activity was seen for low-motility strains. This relationship to motility was investigated by Sengstock *et al* [38]. They proposed that cell division during bacterial proliferation could explain the observed difference in antibacterial activity between

E. coli and *S. aureus*, as *E. coli* multiply by elongating, which requires horizontal movement of the cell body attached to the nanostructures, causing more contact and therefore death, whereas *S. aureus* are able to divide along three planes, resulting in some cell division that does not lead to further contact with nanostructures.

These models and theories informed and directed further research into fabrication of synthetic bactericidal materials, with intent to find the optimal parameters to maximise cell death.

1.3.3 Synthetic mechano-bactericidal materials

Building from the discovery of natural materials, different types of synthetic biomimetic NSS have been investigated for their bactericidal capabilities. Mentioned earlier, titania nanowires fabricated through glancing angle sputter deposition (GLAD) have been shown to exhibit bactericidal properties against *E. coli* [38]. Wu *et al* [39] investigated the performance of gold nanopillars as antibacterial surfaces, showing good performance against Gram-positive *S. aureus*. However, the nanostructured material that has been most thoroughly investigated for this purpose is black silicon.

1.3.4 Black Silicon

Comprised of single wafer crystals of silicon, black silicon (bSi) was originally discovered as an unwanted side effect of Reactive Ion Etching (RIE)[40]. Silicon wafers are etched, typically in a fluorine-containing plasma, resulting in sharp 'needles' where a masking layer has protected the surface. The needle lengths can range from a few microns up to 60 μm, depending on reaction conditions. The term 'black' silicon is used due to the materials extremely low reflectivity – the majority of light is absorbed by the modified Si surface. The highly tuneable nature of this technique for fabrication of an NSS makes black silicon an attractive option for new generations of mechano-bactericidal materials.

Applications of bSi have subsequently been discovered, most notably the material's bactericidal capabilities, hypothesised to be analogous in mechanism to the previously discussed naturally occurring materials. Ivanova *et al* first began investigations into the use of bSi after noting the similarities in structure to the nano-pillared cicada and dragonfly wings[41]. Testing with *S. aureus* cells, they found that bSi (spike length 500 nm) produced comparable cell death rates to *D. bipunctata* wings (spike length 230 nm) – both averaging close to 450,000 cells min^{-1} cm^{-2}.

Since then, bSi has also been proven to display antibacterial properties *in vivo,* the first synthetic biomimetic material to do so[42]. Implanting the black silicon substrate in mice showed that the nanostructured surface produced minor tissue reaction, whereas a smooth, nontextured silicon induced a greater inflammatory reaction.

However, a drawback to the usefulness of bSi as an antibacterial material is its delicacy. The silicon spikes are very brittle due to the low aspect ratio, meaning that under even relatively small forces, the spikes are crushed or broken off from the base. Not only does this destroy the structure and hence any bactericidal tendency, it is also a safety concern, with the very small Si pillars raising asbestos concerns. Thus, if bSi spikes were able to be coated in a material such as diamond, allowing its durability to be improved while still retaining its performance due to the non-specific mechanism, this would greatly increase the potential real-world applications of the composite material.

1.4 Synthetic Diamond

Diamond is an allotrope of carbon comprising of a covalent network of sp^3 hybridised carbon atoms in a tetrahedral lattice. The hardest known material, diamond has long attracted interest in scientific research due to its remarkable properties – chemical inertness, high thermal conductivity and optical transparency. These properties lead to applications such as cutting tools and optical lenses and as inert coatings to improve durability of materials.

Naturally, diamond forms underground when carbon is exposed to extremely high temperatures and pressures. Synthetic diamond was first synthesised by mimicking these natural conditions, and the HPHT method was established. This method of diamond production however is not ideal due to the extreme conditions required, and the limitation that only single crystals of diamond can be formed in this way. This lead to the realisation of a new technique for diamond growth – Chemical Vapour Deposition.

1.4.1 Chemical Vapour Deposition

Chemical Vapour Deposition (CVD) has now become the more favoured method for diamond thin film fabrication, due to the relatively low pressures required, as well as the ability to grow larger areas of continuous diamond. First investigated in 1958[43], it consists of a step-by-step approach of adding carbon atoms to a surface in such a way that the tetrahedral sp^3 structure can be built.

The process involves the diffusion of methane and hydrogen towards a surface, during which they undergo activation. The gases fragment and form radicals which participate in a series of reactions at the surface to gradually deposit diamond. Atomic hydrogen is key in this process - H radicals react with terminal C-H bonds in the diamond structure to form hydrogen, which creates a vacancy on the surface. Hydrocarbons can then react at the site, creating an additional C-C bond resulting in growth of the diamond lattice, or atomic H can re-populate the vacancy and the diamond is preserved[44]. It also preferentially etches away graphitic sp^2 carbon that is deposited and leaves only sp^3, and

terminates the 'dangling' C- bond left at the surface, preventing cross-linkage. Excess hydrogen (99%) in the gas mixture ensures complete hydrogen termination of the surface[45].

Activation of the gases can be achieved either through thermal decomposition, brought about by heating of the gases to thousands of Kelvin, or through electrical discharge. These two methods correspond to the most prevalent diamond CVD techniques – Hot Filament (HF)-CVD and Microwave plasma (MW)-CVD[46]. Figure 6 illustrates the conditions within the growth chamber of a HF-CVD reactor.

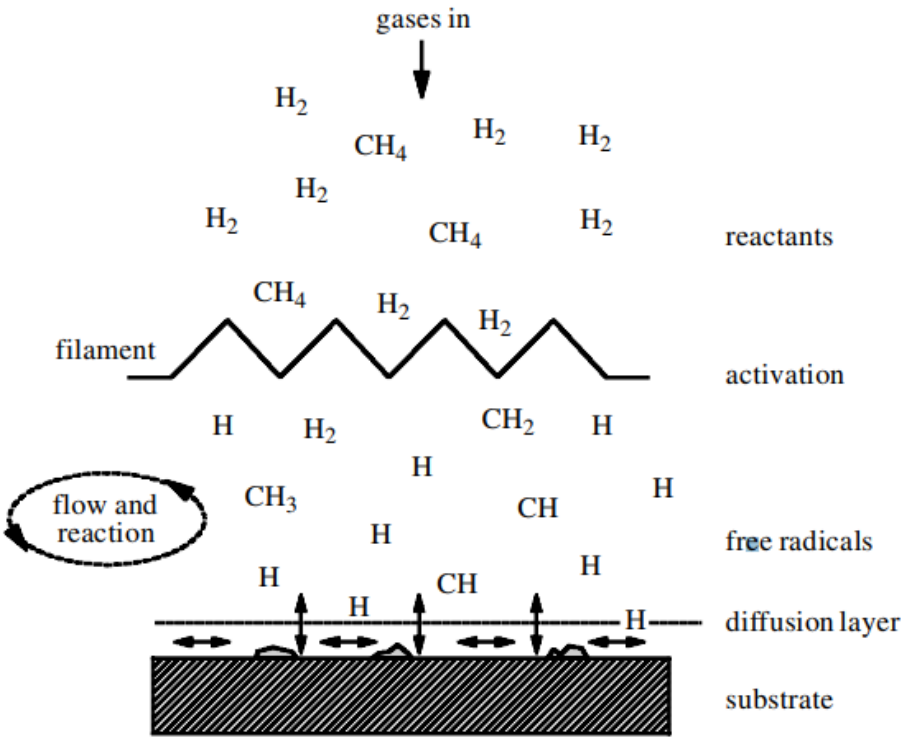

Figure 6 - Diagram detailing the process involved in HF-CVD diamond growth [46].

1.4.2 Surface modification

The surface chemistry of diamond films can be modified by replacing terminal hydrogens (Figure 7) from surface C-H bonds with other elements or molecules[47]. This can be done to provide additional functionality to the diamond film by altering properties such as hydrophobicity, electron affinity and conductivity.

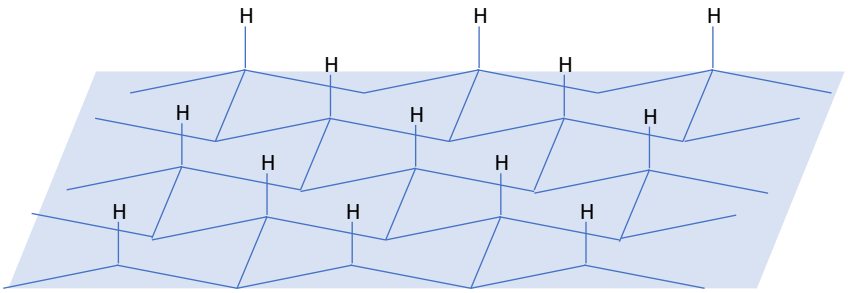

Figure 7 - Diagram illustrating the presence of 'dangling' C-H bonds on the surface of a diamond film that are replaced by surface termination. For clarity, internal C-C bonds are omitted.

Oxygen terminated diamond films can be produced by exposure to an oxygen plasma, or UV irradiation in air for a sufficient length of time[48]. This results in replacement of terminal hydrogen with carbonyl, carboxylic acid and alcohol groups, increasing surface hydrophilicity. Amino-terminated diamond surfaces can also be created in ammonia plasma environments[49], resulting in replacement of terminal hydrogen with NH_2 groups.

Fluorine containing gases have also been used to terminate diamond, as a method of providing surface functionality and increased hydrophobicity, with potential applications in biosensors [50] and electrochemistry [51]. Ray *et al* successfully used CF_4 containing plasma to generate 50% surface fluorination of diamond films, and FTIR was used to confirm the presence of CF_2 and CF_3 bonds[52].

Relating to applications in bactericidal materials, research has shown that oxygen-terminated diamond allowed for increased cell adhesion and subsequent growth on the surface when compared to H-terminated[53]. This was attributed to the increased deadhesion forces resulting from increased hydrophilicity, and the presence of carbonyl and carboxylic acid groups, leading to stronger hydrogen bonding interactions between cell membrane proteins and the diamond surface. Although this research was carried out with the focus on applications for cultivating cell growth, it can be envisaged that if this increased cell adhesion through a chemical mechanism can be combined with physical bactericidal mechanisms, a surface that attracts bacteria to it and then destroys it on contact could be possible.

Conversely, creation of a surface that makes use of its hydrophobicity to repel bacteria and reduce attachment in the first instance, whilst also destroying any cells that do come into contact, would theoretically combine the benefits of bacteria-resistant and bactericidal surfaces.

1.5 PRIOR WORK

Prior work based at the Universiry of Bristol has begun to investigate diamond coated bSi for bactericidal applications. HF-CVD was established as a viable method for diamond-coating of bSi. Cell death of Gram-negative *P. aeruginosa* on diamond coated bSi of needle length 0.5-1.0 µm was established at 13%; an improvement compared to 2% for a control flat diamond film[54]. Visual imaging of the cells on the flat *vs* NSS revealed that when incubated on the needles, cells became flat and lost their uniform cylindrical shape, indicative of membrane rupture.

Research was then expanded to *E. coli* bacteria, which was trialled with 3 lengths of bSi: 0.5 µm, 2.5 µm and 20 µm. Cell death rate on the uncoated needles was increased by a maximum of 25% compared to a flat Si control, obtained by the shortest needles. However, these needles were unable to be coated with a diamond film, as the growth duration required to form a continuous coating resulted in the diamond film completely overgrowing the needles and removing the nanostructure. The 20 µm needles were diamond coated, and bactericidal activity was not found to have any significant increase compared to a flat diamond surface, with a cell death of 23% and 20% respectively[55].

The main property that was observed to affect cell death was spike density, with the more densely packed needles performing better. This was theorised to be due to the less dense needles allowing bacteria to sink down between spikes, thus avoiding contact with the needle tips.

1.6 PROJECT AIMS

This project aims to build on the prior work of the Bristol Diamond Group detailed in the previous section; to increase the understanding of the bactericidal activity of black silicon and the effect that diamond coating has on its performance and durability.

This will be achieved by thorough investigation of bSi of a new needle length and density, to add to the existing database and help to establish the effect that needle density, needle height and tip diameter have on bactericidal performance. The relationship between cell death and available surface area (SA_{Av}) of a surface, a parameter that considers both tip diameter and density will be examined. The length of bSi needle to be focused on is in-between the previously studied 20 µm needles that were found to be insufficiently dense, and the short 0.5 µm needles that were too short to be successfully diamond coated.

Secondly, the effect of surface hydrophobicity on bacterial adhesion and cell death rate will be investigated, to establish if chemical composition plays any role in degree of cell death and to determine if the properties of bacteria-resistant and bactericidal materials can be combined in such a way to significantly increase efficacy.

2 METHODS

2.1 BLACK SILICON

The bSi samples were provided by Colin Welch at Oxford Instruments Plasma Technology. The samples were cut to squares of area 1 cm^2 using a diamond scribe before further processing.

2.2 SEEDING

Prior to diamond growth, the bSi samples were seeded with nanodiamond to increase initial nucleation rate. A nanodiamond suspension consisting of NanoAmando colloid (10 drops) in methanol (~ 25 mL) was creating using probe sonication (1 hr). The suspension was applied to the surfaces using electrospray technique. Samples were attached to a grounded rotating disc (60 rpm) and the suspension fed through a charged needle (65 kV), allowing atomisation of the suspension and evaporation of the solvent as it travelled to the disc to deposit a regular distribution of nanodiamond clusters. The efficacy of the seeding process was confirmed using optical microscopy.

2.3 DIAMOND GROWTH

The seeded samples were placed in the HF-CVD reactor and the chamber evacuated to between 1.0-2.0 x 10^{-2} Torr before initiating growth. Growth conditions were 1 % CH_4 in H_2 (flow rates of 2 sccm and 200 sccm respectively), with pressure maintained at ~ 20 Torr. A current of 25 A was supplied using Ta filament wire, which gave rise to a voltage of 7-9 V and a gas temperature of ~ 1000 K each run. Runs were kept to 1 hr in duration, with CH_4 supply turned off for 1 min before run termination to ensure H-termination of the surface bonds.

Control samples of diamond films grown on flat p-type (<100>) Si wafers were fabricated following the same seeding and growth conditions, except for extension of the growth duration to 8 hr to ensure a continuous film coating.

2.4 CHARACTERISATION

2.4.1 Microscopy

Samples were characterised using Scanning Electron Microscopy (SEM) and Transmission Electron Microscopy (TEM). Images obtained were analysed using ImageJ software to determine needle dimensions and density.

2.4.2 Raman spectroscopy

Raman spectra of the uncoated and coated bSi surfaces were obtained at room temperature using a Renishaw 2000 Raman spectrometer. The samples were excited using an argon-ion laser (λ = 515.5 nm, green light).

2.4.3 Surface hardness

Qualitative assessments of the mechanical and thermal resistance of bSi and D-bSi were carried out. Surfaces were manually scratched using tweezers at different applied forces, and thermally etched using an Oxford Lasers laser cutter.

2.5 Surface Termination

To alter the surface chemistry of the diamond coated bSi, samples were exposed to plasmas of 3 different gases: O_2, NH_3 and SF_6, using a modified sputter coater apparatus. Samples were placed in contact with an anode and sealed in an airtight chamber, with a rotary pump creating a base pressure of 7 x 10^{-3} Torr. The desired gas was then supplied to the system at a flow rate of 10 sccm, and a voltage applied to the system to generate a plasma. The optimum conditions for creating a plasma with each gas, as well as the exposure times before the voltage was turned off are detailed in Table 1.

Table 1 - Conditions for optimum plasma generation for surface terminations of D-bSi

Gas	Pressure / Torr	Voltage / V	Exposure duration / s
O_2	0.1-1.5	4-9	8
NH_3	1.3-1.6	7-9	60
SF_6	0.1-0.3	7-9	10

The resulting 4 surfaces are henceforth referred to as H-, O-, NH_2-, and F-terminated D-bSi.

2.6 Contact Angle (CA) measurement

Terminations of the diamond films and hence differences in hydrophobicity were confirmed by water CA measurements. Samples were washed with ethanol and air dried before testing using a Krüss droplet shape analyser in combination with Advance software. 5 µL droplets were pipetted onto each surface whilst the program recorded the contact angle at 1 s intervals until the value stabilised. Due to limited supply, CA of NH_3-terminated surfaces was unable to be measured.

2.7 BACTERIA LIVE/DEAD ASSAY

To prepare the bacterial suspensions, *E. coli* (strain DH5-α) stock (37.5 µL) was added to Tryptic Soy Broth (TSB, Oxoid) (15 mL) and grown under aerobic conditions in a static shaker for 16 hr. The suspension was then added in intervals to autoclaved TSB (25 mL) until an optical density (OD_{600}) of 0.1 was reached. The suspension was further incubated until mid-exponential phase was reached (OD_{600} = 0.5), upon which the bacterial cells were harvested by centrifugation (7 min, 5000 g) and washed with tris-HCl buffer (10 mM, pH = 7), before suspending in buffer to reach OD_{600} = 0.3. All surfaces to be treated with *E. coli* were washed with EtOH and air dried, before submerging in the bacterial suspension (2 mL) in a 12 well microtitre plate and incubating under static conditions (37 °C, 1 hr).

Samples were rinsed with tris-HCl buffer (3 x) to removed non-adherred cells. BacLight Live/Dead viability stain was made up according to manufacturer's instructions, and samples were incubated in the stain (1 mL) for 15 min at 21 °C in darkness. Finally, samples were rinsed with buffer before observing using fluorescence microscopy.

To determine live/dead count, 4 images of each surface were taken (magnification x20, each corresponding to an area of 0.097 mm^2), and live (SYTO9, green) and dead (propidium iodide, red) cell counts were recorded using ImageJ software.

2.8 SEM PREPARATION

On completion of Live/Dead assays, bacteria were fixed on samples overnight using glutaraldehyde (2.5%) at 4 °C. Samples were then washed in buffer (0.1 M) and dehydrated using graded ethanol series (20%, 50%, 70%, 90%, 100%, 10 min each), followed by critical point drying, and Au-sputter coating before observation.

3 RESULTS AND DISCUSSION

3.1 CONTROL SURFACES

3.1.1 Uncoated bSi

The specific sample of bSi chosen to be the template for diamond growth was selected for a number of its properties. As shown in Figure 8, the needle lengths have a larger variation than previously examined bSi samples (Figure 9). The average needle length was bimodal, analogous to the previously described dragonfly wings, which in theory would help to minimise the 'bed of nails' effect, as well as increase the potential for cells to be destroyed *via* the proposed mechanism that Bandara *et al* described [30].

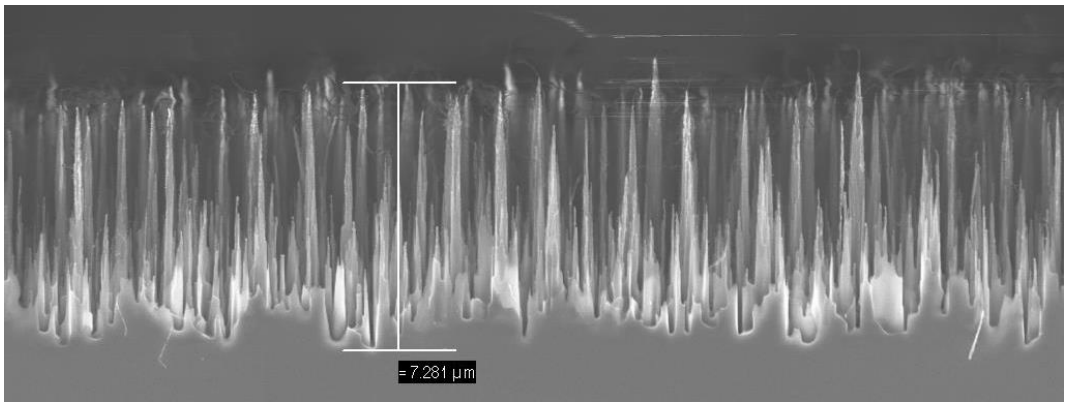

Figure 8 - SEM image of the chosen bSi sample, with maximum needle height indicated.

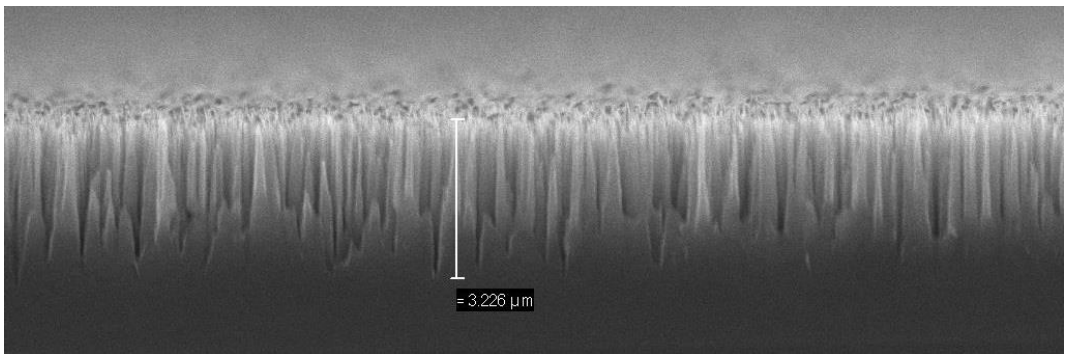

Figure 9 - SEM image of bSi previously used for bactericidal testing, with max. needle height indicated.

3.1.2 Flat diamond film

Growth of diamond on a seeded flat silicon wafer according to the growth conditions detailed in section 2.3 resulted in a continuous diamond film shown in Figure 10. As can be seen the grain size of the diamond crystal varies from a few 100 nm to 1 µm, indicating polycrystalline diamond. It should also be noted that although the sample is referred to as 'flat' for comparison to the needle coated surfaces, it is actually a faceted surface that still possesses some degree of surface texture.

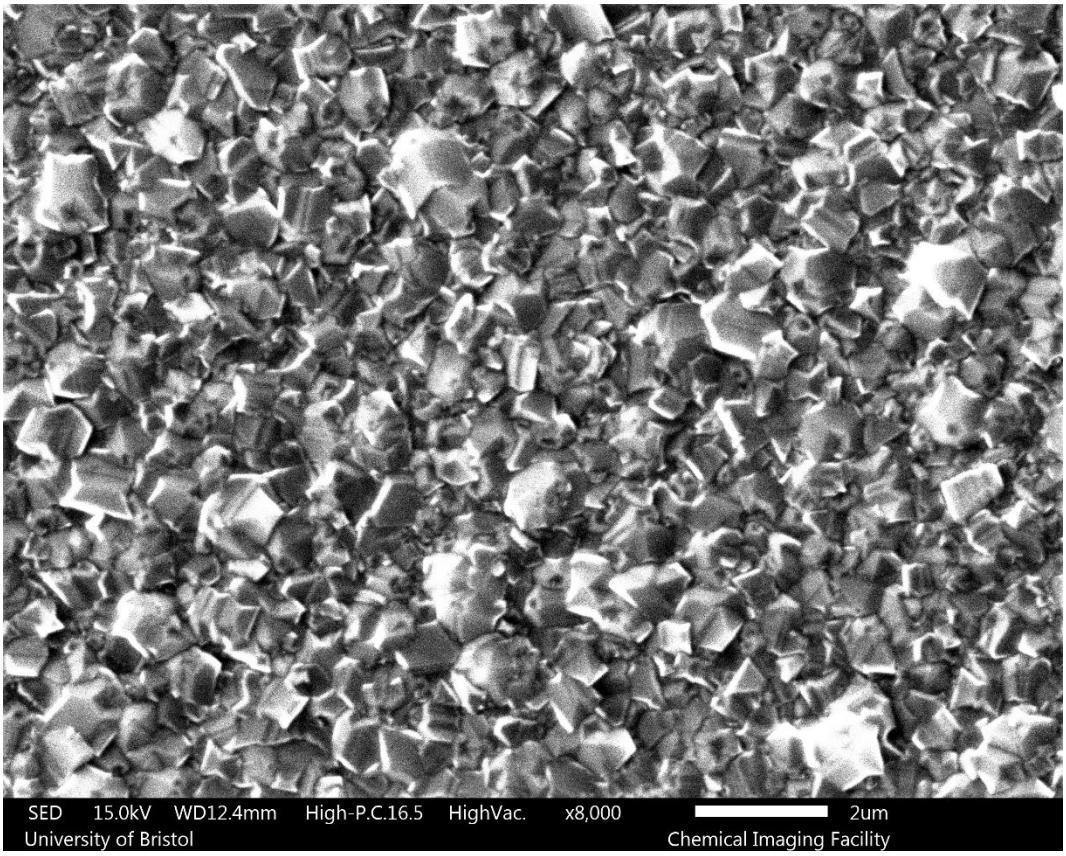

Figure 10 - SEM image of top-down view of control 'flat' diamond film, grown for 8 hours (mag.x8000).

3.2 DIAMOND COATING OF BLACK SILICON

SEM and Raman spectroscopy were used to characterise the D-bSi. The diamond growth conditions employed were shown to repeatedly produce diamond-coated black silicon (D-bSi) needles, the surface morphology of which is shown in Figure 12 compared to the uncoated bSi shown in Figure 11. 1 hr of growth resulted in a continuous diamond coating, which lead to an increase in average tip diameter of the needles by 277 nm (Table 2). However, the average needle length was reduced by over a micron, indicating that during the growth some of the silicon was initially etched away by the

process gases before diamond deposition began. Needle density was reduced slightly upon diamond coating, indicating that some Si spikes merged together as the diamond coating grew. Examples of needle merging are indicated in Figure 12.

Although a uniform film was fabricated, it can be observed from SEM images that at the base of the needle there is a section approx. 0.5 µm in length that is uncoated, with the silicon exposed. This could be due to the seeding process of diamond deposition unable to reach this far down into the nanostructure, or coalescing of the diamond film above this point, rendering it unable to coat the small crevices.

Table 2 - Summary of observed properties of uncoated bSi compared to diamond coated bSi (D-bSi)

Sample	Tip diameter / µm	Length / µm	Needle density ξ / µm^{-2}	SA_{Av}
bSi	0.059 ± 0.021	4.62 ± 1.51	1.43	0.004
D-bSi	0.336 ± 0.063	2.98 ± 1.27	1.20	0.106

As stated in Table 2, an additional parameter for inter-surface comparison has been included. The fraction of available surface area (SA_{Av}/A_0) is a parameter that accounts for the variation in tip diameter and needle density parameters simultaneously. It can be defined as the fraction of surface area per unit area that is available for contact with bacteria upon onset of adhesion compared to a flat surface, expressed as $\frac{SA_{Av}}{A_0} = \pi r^2 . \xi$. For a flat surface, this ratio will be 1, as the entire surface area is available. However for an NSS, if it is assumed that the only point of contact with the bacteria is the needle tip (assumed as a flat circle for simplicity), this fraction is reduced with reduced tip diameter and reduced density. Another way of looking at this parameter is as a much simpler indication of the stretching degree a cell will experience on contact with an NSS. The lower the value of $\frac{SA_{Av}}{A_0}$, the higher the proportion of the cell membrane surface area that is suspended between points of contact, leading to an increase in potential stretching degree, which is modelled to lead to cell deformation. For conciseness in this report, the given area A_0 will always be 1 µm², and $\frac{SA_{Av}}{A_0}$ will be quoted as SA_{Av} with units of µm^2.

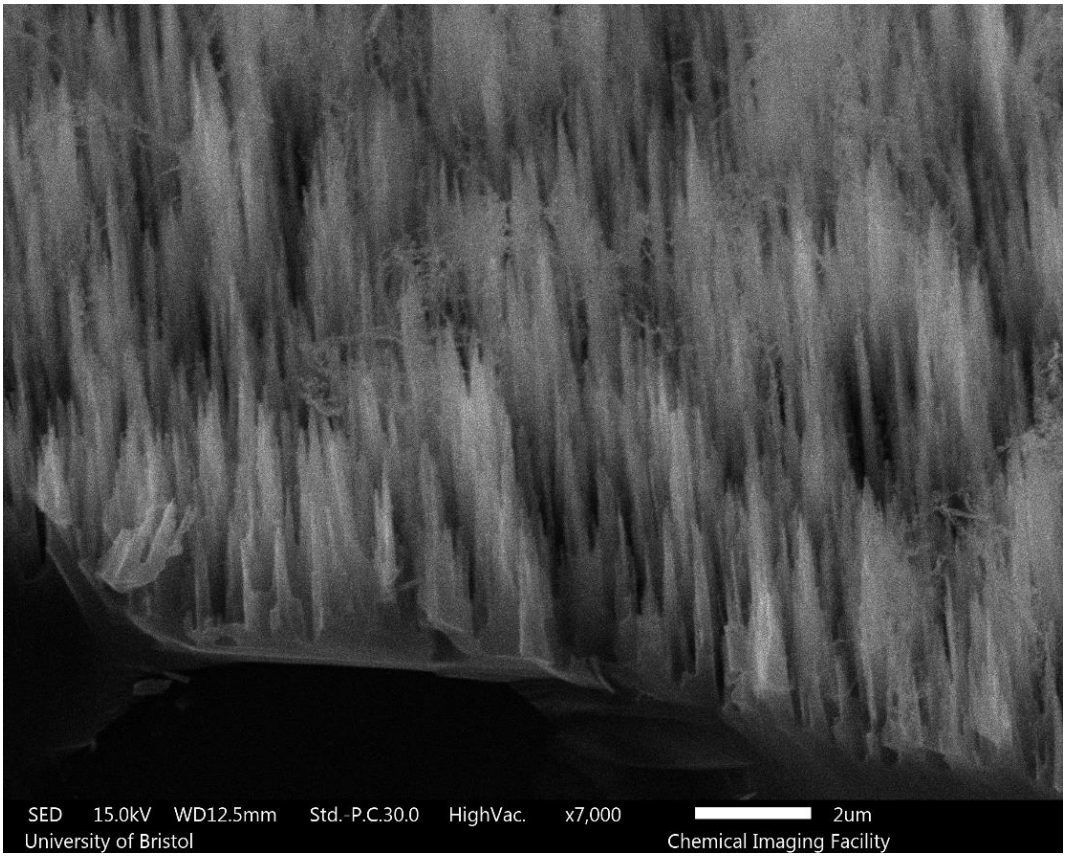

Figure 11 - SEM image of uncoated bSi spikes of average length 4.6 µm, mag. x7000, 45°

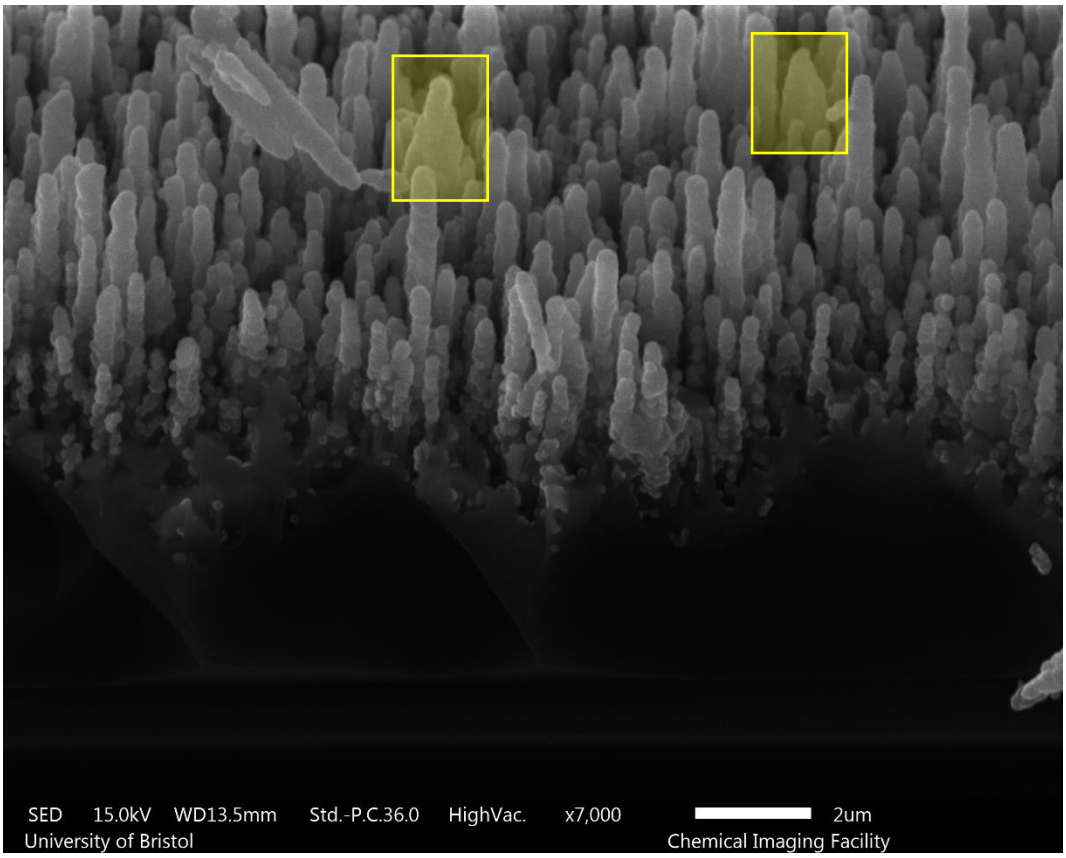

Figure 12 - SEM image of bSi spikes after 1 hr growth of diamond, average length 3.0 µm, mag. x7000, 45°. Instances of spike merging leading to lower spike density are indicated.

TEM images also indicated that silicon is etched before deposition, with the silicon core of the coated needle shown to be only ~32 nm in diameter (Figure 11), compared to the average of ~ 60 nm for the bSi before growth. This suggested that the growth process favourably etched the Si spikes in the vertical direction.

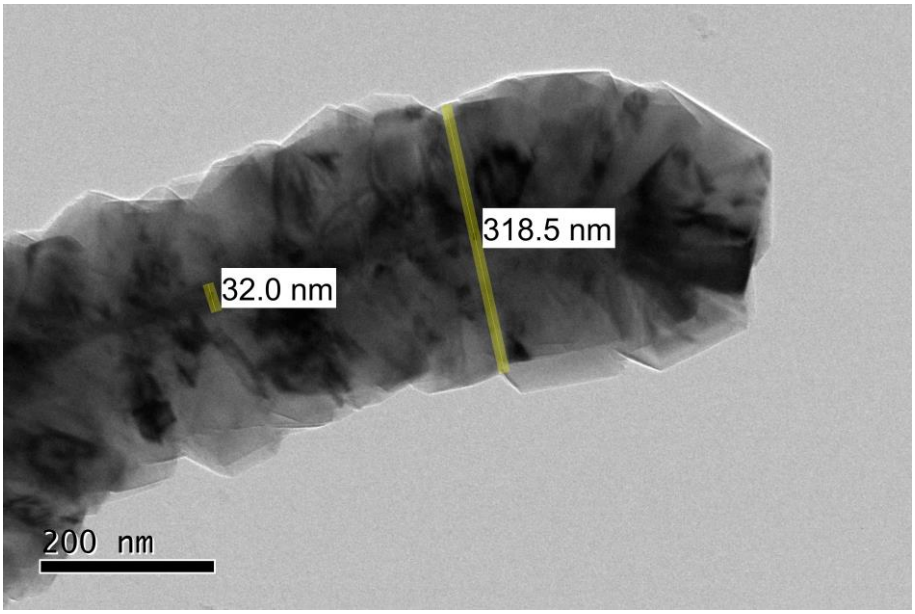

Figure 11- TEM image of D-bSi

As shown in Figure 12, Raman spectra indicated that the growth conditions employed resulted in an impure diamond film. Graphitic sp^2 carbon was present in the D-bSi, indicated by the characteristic D and G broad peaks at 1367 cm^{-1} and 1559 cm^{-1} respectively, as well as impurity peaks at 1137 cm^{-1} and 1466 cm^{-1}, which Ferrari *et al* have attributed to transpolyacetylene present at grain boundaries[58]. None of these impurities are observed in the seeded bSi spectrum, which only features the characteristic sp^3 diamond shift at 1332 cm^{-1}, and the 1st and 2nd order Si peaks. All of these peaks, collated in Table 3, are commonly observed in CVD diamond films, and an impure film was to be expected, given the short growth time and the mechanism of CVD diamond deposition – the longer the growth cycle, the more sp^2 carbon is etched away, and the better the diamond quality. The spectrum observed is comparable to those observed for nanocrystalline diamond films, where the reduced crystallite size results in a larger concentration of grain boundaries and hence different phases of carbon[56].

Table 3 - Summary of peaks observed in Raman spectrum of CVD diamond films, comparing literature values to those obtained for DbSi [57,58]

Assignment	Raman shift / cm^{-1} Literature	Experimental
1st order Si	520	519
2nd order Si		970
Grain boundary transpolyacetylene	1100-1150	1137
sp^3 first order	1332	1332
sp^2 amorphous 'D band'	1345	1367
Grain boundary transpolyacetylene	1430-1470	1466
sp^2 amorphous 'G band'	1520-1580	1559

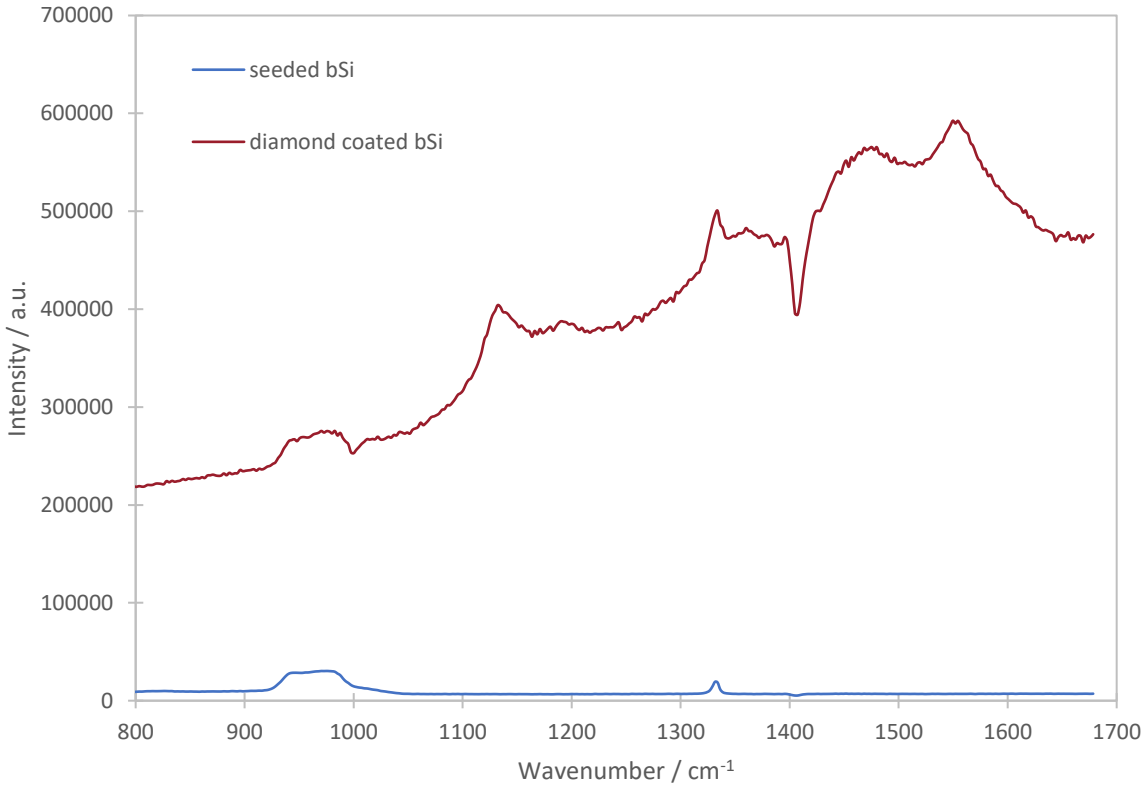

Figure 12 - Obtained Raman spectra for the nanodiamond seeded bSi surface and the 1 hr growth D-bSi. The 1st order Si peaks at 519 cm^{-1} are omitted for clarity.

3.3 MECHANICAL TESTING

Visual comparisons of the effect of mechanical scratch tests on bSi and D-bSi are shown in Figure 13. Although no quantitative comparisons can be made, upon inspection, it appears destruction of needles for both surfaces occurred to a similar extent. This indicates that diamond coating provided no improvement to the durability of bSi. This can be attributed to a number of factors. A diamond coating of thickness of ~300 nm is insufficient to produce a tangible improvement to durability, especially with the knowledge that it is impure. In addition to this, the bSi left exposed at the base of the needle is a weak point of contact, meaning any force acting on this area will result in shearing of the needle from the wafer base.

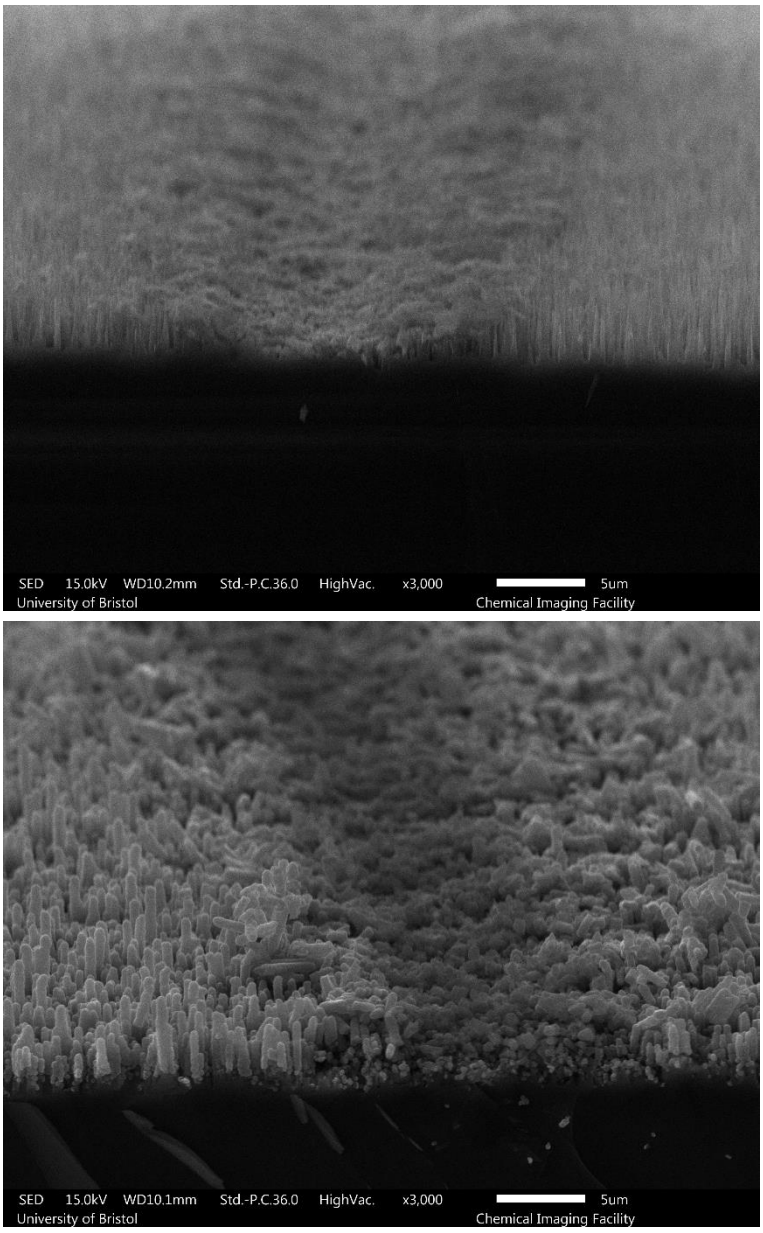

Figure 13 - SEM images of scratch surfaces of bSi (top) and D-bSi (bottom) surfaces, mag. x3000

3.4 Surface Termination

Water contact angle measurements were used to confirm that the plasma conditions employed for surface termination were successful. The contact angles are summarised in Figure 14. Contact angle of the flat control diamond film was recorded as 84.8°, in agreement with previously reported literature values[47], with uncoated bSi exhibiting a very similar CA of 83.8. However, by comparison the contact of water with the bSi surface was shown to be a dynamic process, with the contact angle steadily decreasing over time as the liquid spread into the nanostructure, common for surface the exhibit large degrees of surface roughness.

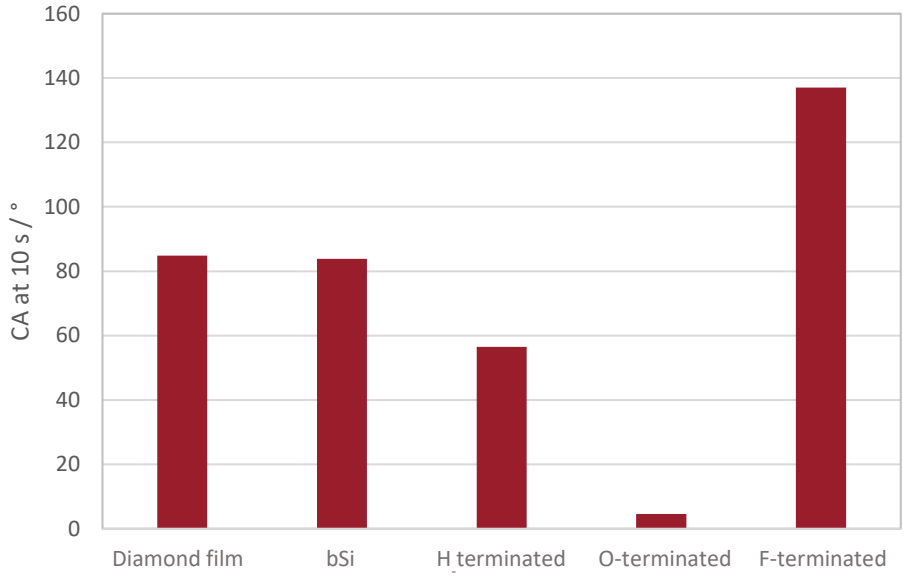

Figure 14 - Water contact angles obtained after 10 s for each surface.

O-termination of the D-bSi led to a large increase in wettability of the surface, with the contact angle reduced from 56.5° for H-terminated to 4.6°. Conversely, F-termination caused the contact angle to increase to 137.0°. Visual differences in water droplet shape are illustrated in Figure 15.

The observed changes in contact angle for the O-terminated and F-terminated films are much more extreme than previously reported values of - 8° for O-terminated and + 10° for F-terminated flat diamond films compared to H-terminated[47], suggesting that conditions employed for termination resulted in a more thorough replacement of C-H bonds than literature method. However, direct comparisons cannot be made due to only flat diamond surfaces being characterised; no prior research has involved termination of D-bSi. The increased effect was attributed to the increases surface roughness of the NSS compared to the flat. In addition to this, a possibly theory is as a result of the increase in exposed diamond surface area that results from diamond coating bSi, meaning by area, the nanostructured diamond needles will have more dangling bonds available to react with the terminating gases, providing a higher concentration of new terminations.

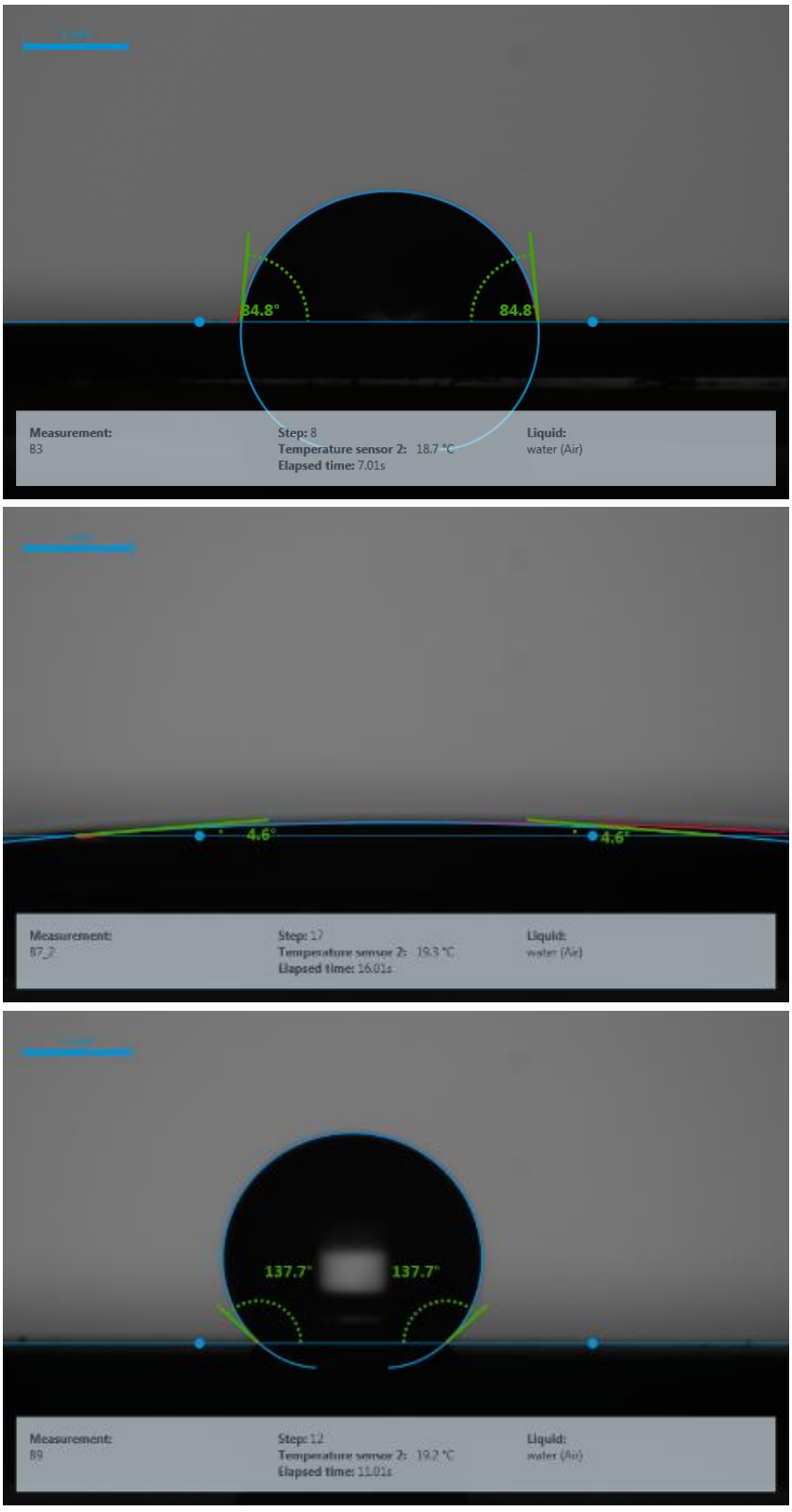

Figure 15 - Visual comparisons of the obtained water contact angles of a) H-terminated, b) O-terminated and c) F-terminated D-bSi

3.5 BACTERICIDAL ACTIVITY

For the scope of this project, it was decided to focus on a Gram-negative strain of bacteria, as literature has established this type to be the more susceptible to mechano-bactericidal attack. The harmless DH5-α strain of *E. coli* bacteria was selected for ease of cultivation and availability. The Live/Dead staining procedure allowed for quantification of viable cells. It is comprised of two fluorophores; SYTO9 and propinium iodide (PI). SYTO9 is able to enter both live and dead cells and the green fluorescence is enhanced upon intercalation with DNA. PI, however, can only penetrate the disrupted cell membranes of dead cells, displacing SYTO9 due to its higher binding affinity to DNA, resulting in red fluorescence for dead cells.

The obtained cell death ratios and total cell counts for D-bSi compared to the two controls is displayed in Figure 16. Flat, polished Si wafers were also tested, but the surface was found to be too smooth, and negligible cell adhesion was observed.

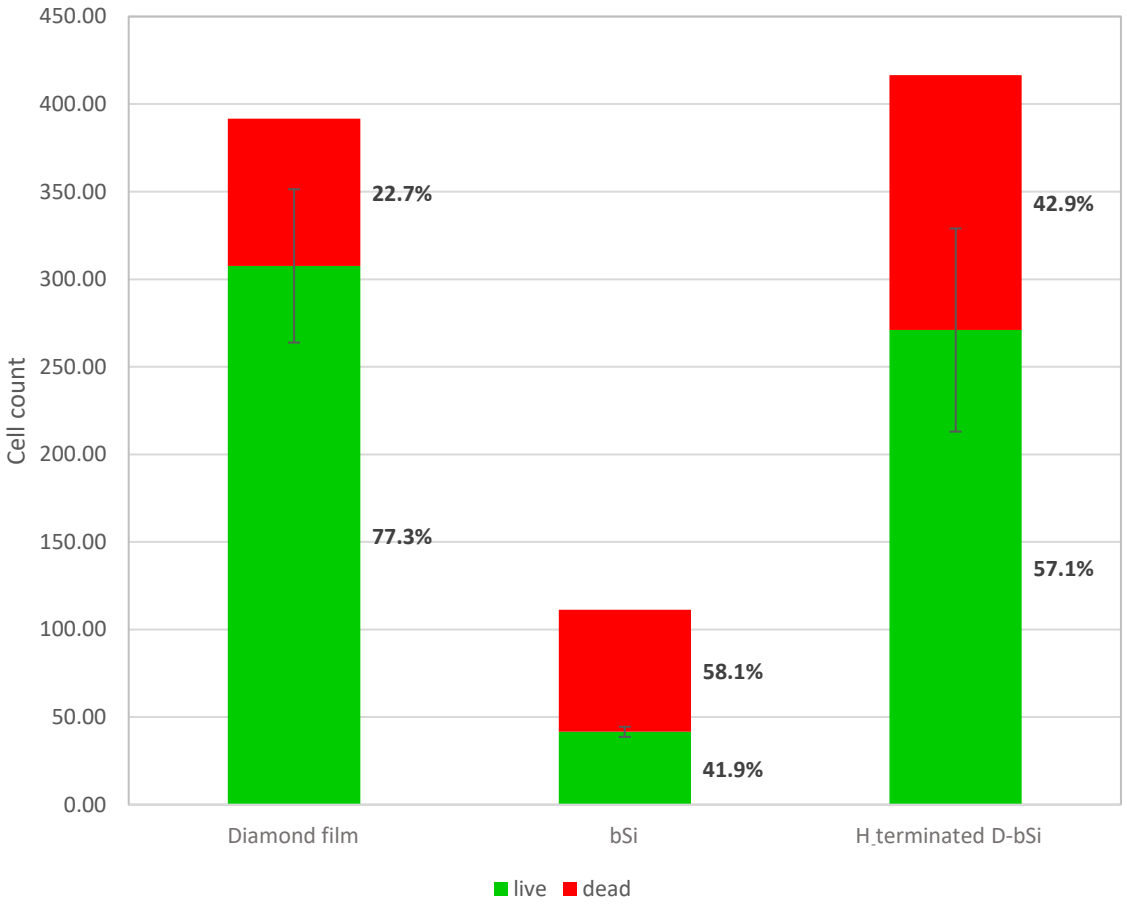

Figure 16 - Graph displaying average cell live/dead ratios and total cell adhesion across all surfaces. Error bars are shown as standard deviation of the cell death percentage.

3.5.1 Impact of nanostructuring

Comparing the flat diamond film to D-bSi, the cell death percentage increased by 20.2% from the flat to nano-structured diamond surfaces. This improvement was expected, and the diamond was grown under the same conditions, it can be stated that the only difference between the two surfaces is the topography of the surface. This supports the theory of nanostructures imparting stress on cell membranes due to suspended surface area and hence death.

Total cell adhesion was comparable, with average cell count showing a small from 392 to 417 for the D-bSi, indicating that surface nanostructuring did not have any significant impact on ability of bacteria to adhere to the surface. This is an indicator that the physical differences in the topography of the surface, manifested in surface roughness and SA_{Av} have less impact on cell adhesion when compared to the chemical composition of the surface.

3.5.1.1 Biofilm formation

A qualitative observation made from the obtained fluorescence microscopy images was the reduction in the onset of biofilm formation on the nanostructured surfaces. Clusters of live bacteria cells as seen in Figure 17 and visualised in Figure 18 appeared more frequently on the flat diamond control than on the needle-coated surfaces. This was attributed to the differences in SA_{Av}. On the continuous flat surface, bacteria cells were able to settle at any given location, whereas on the NSS, the horizontal surface area is discontinuous and SA_{Av} is reduced, resulting in a finite number of possible points for bacteria to adhere. This worked to minimise the potential for bacteria clustering and division, two essential processes in onset of biofilm formation.

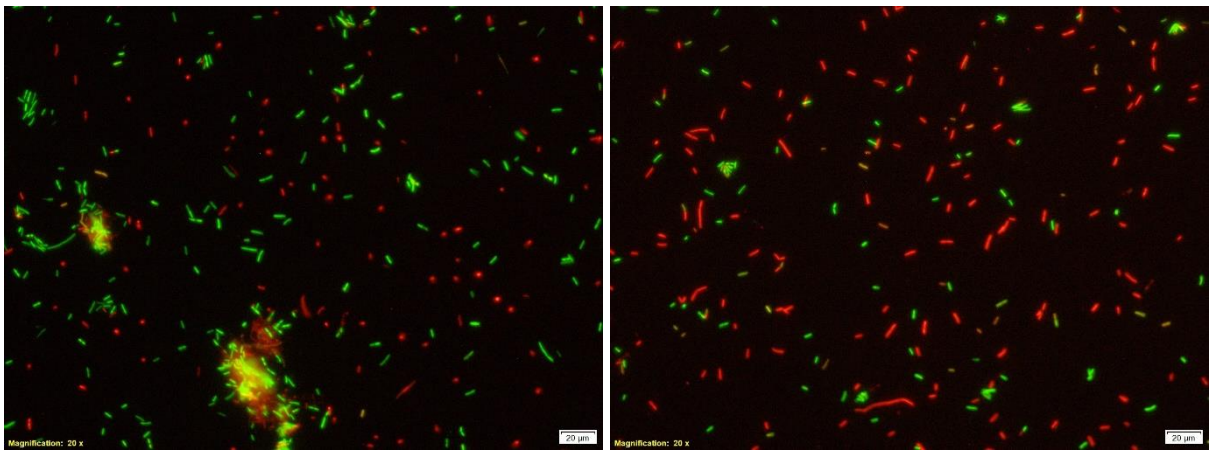

Figure 17 - Fluorescence microscopy images of flat diamond thin film (left) compared to bSi (right), showing the reduction in live cell aggregates caused by the nanostructures.

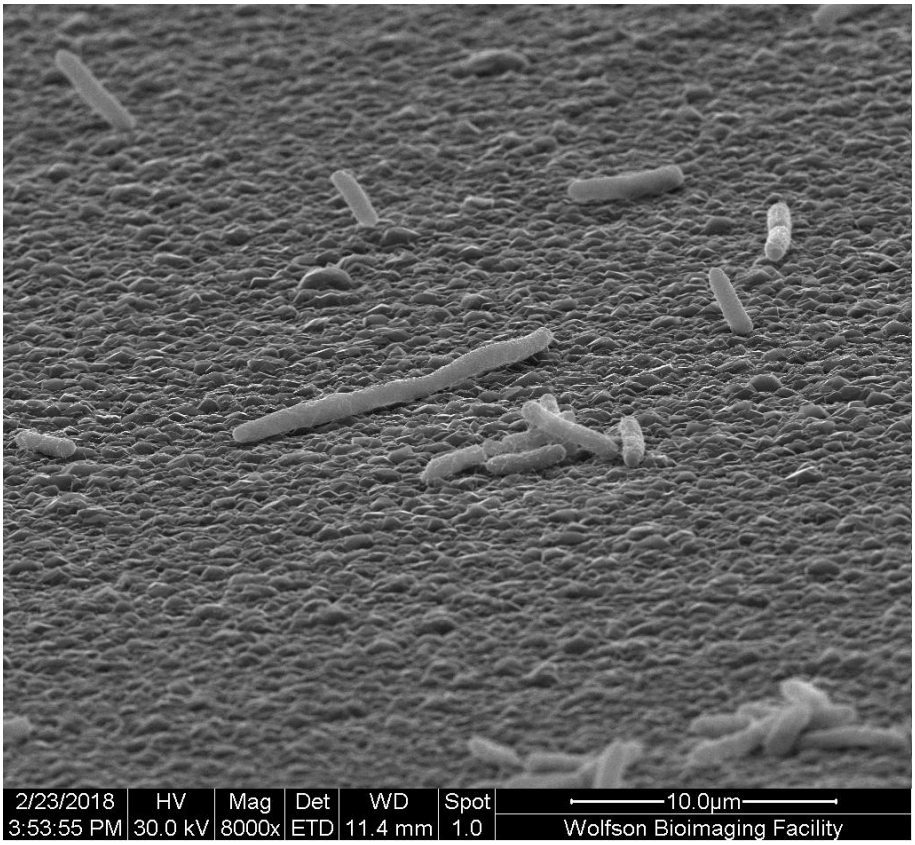

Figure 18 - SEM of bacteria cells adhered to flat diamond film, showing instances of cell clustering

3.5.2 Impact of diamond coating

The uncoated bSi was found to have an average cell death percentage of 58.1%. The effect of diamond coating on the performance of bSi resulted in a reduction in average cell death by 15.2%. Assuming cell death mechanism to be purely physical, the most prominent change that occurs on diamond coating is the increase in tip diameter, and hence SA_{Av}, so the reduction in bactericidal efficacy was attributed to this.

Cell adhesion however increased 4-fold upon diamond coating, with H-terminated D-bSi exhibiting the highest cell adhesion. Again, a reason for this could be the larger horizontal surface produced by addition of diamond to the spikes, but this difference in cell adhesion observed upon altering the surface chemistry of the NSS shows that cell adhesion is also influenced by surface chemistry and the potential interactions that can occur.

3.5.3 Effect of SA_{Av}

Comparing the cell death percentage of 58.1% for bSi to those previously obtained for other bSi samples, this is almost double the best performing sample at 31%. Comparison of these results when considering tip density (1.4 μm^{-2} and 65 μm^{-2} respectively) shows the inverse relationship to what has

previously been established between cell death and tip density. To further elucidate the reasoning for this difference, available data on bSi samples of varying tip diameter and density was compiled to establish if there is a relationship between cell death percentage and SA_{Av}. The data is displayed in Figure 19. Despite a very small data set, an overall trend of decrease in cell death with increase in SA_{Av} can be seen. This implies that the larger the surface area of cell membrane in contact with the needles, the less likely it is to be destroyed. However this is an overly-simplistic correlation that ignores many other factors, and more data points would need to be examined before conclusions could be drawn.

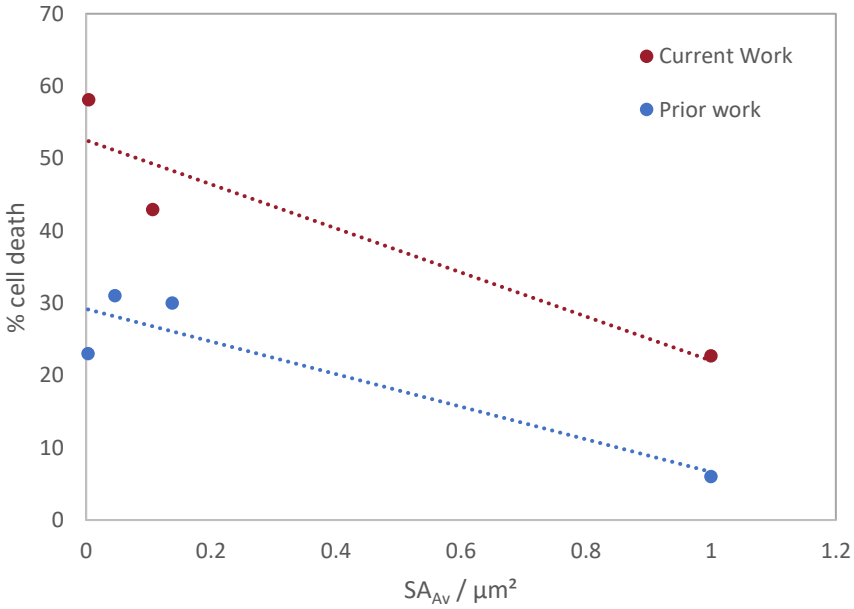

Figure 19 - Graph showing the relationship between cell death percentage and available surface area. Prior work data compiled from [55]

The other main difference in structure of bSi needles that could cause this large increase in cell death is the bimodal needle height phenomenon present in the bSi investigated in this study. Given lack of trend observed taking into account tip diameter, it is quite possible that variance in height of the potentially adhesion sites results in more frequent contact with other nanospikes as a cell tries to move around and duplicate on the surface, potentially increasing cell death. However, this is just a theory and needs to be investigated under higher scrutiny.

3.5.4 Result repeatability

Due to the variable nature of *E. coli* growth, repeat batches of bacterial suspensions resulted in different cell concentrations and hence total cell count on a given surface. This observation is illustrated by comparing cell adhesions on 4 repeats of bSi control tested with 4 different *E. coli* batches, shown in Figure 20. It is seen that despite wide fluctuations in total cell count, the cell death percentage was independent of cell count, and can therefore be compared across batches. However

for cell count, this comparisons between surfaces were restricted to those that had been tested with the same batch, inter-batch comparison was not possible. Thus, the effects of surface hydrophilicity and hydrophobicity were explored separately, as these surfaces were tested with different *E. coli* batches.

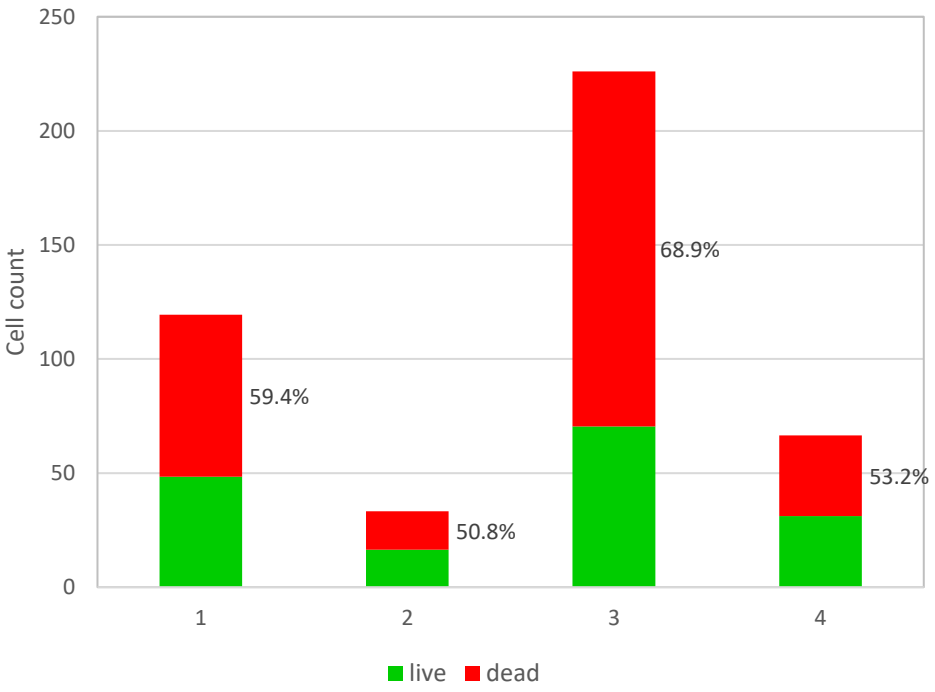

Figure 20 - Live/Dead results of 4 repeats of bSi, shown as fractions of total cell count and as percentage.

3.5.5 Surface hydrophilicity

When comparing the H-terminated to the more hydrophilic NH_2-terminated and O-terminated surfaces, it was observed that increasing hydrophilicity increased cell density for the diamond coated surfaces, with O-terminated D-bSi exhibiting the highest adhesion (Figures 23-24). This is in line with what would be the expected trend of cellular adhesion to diamond materials, with the addition of

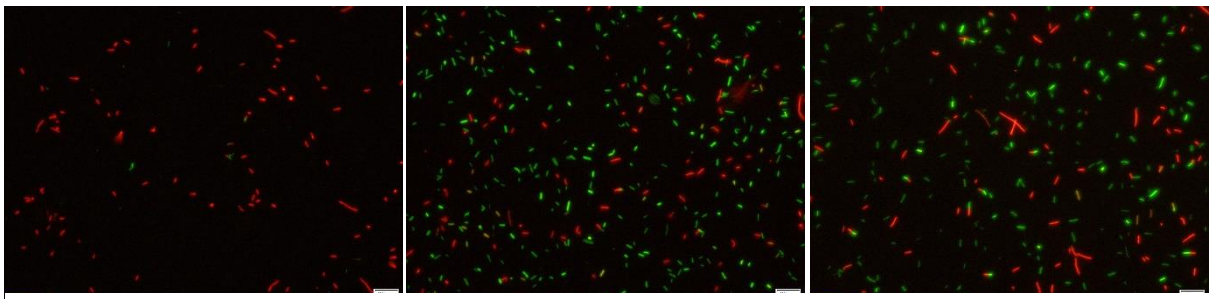

Figure 21 - Fluorescence micrographs showing differences in cell adhesion across different surface terminated diamond films

amine and oxygen-contained groups leading to stronger attractive hydrogen bonding interactions between cell membrane proteins and the diamond surface.

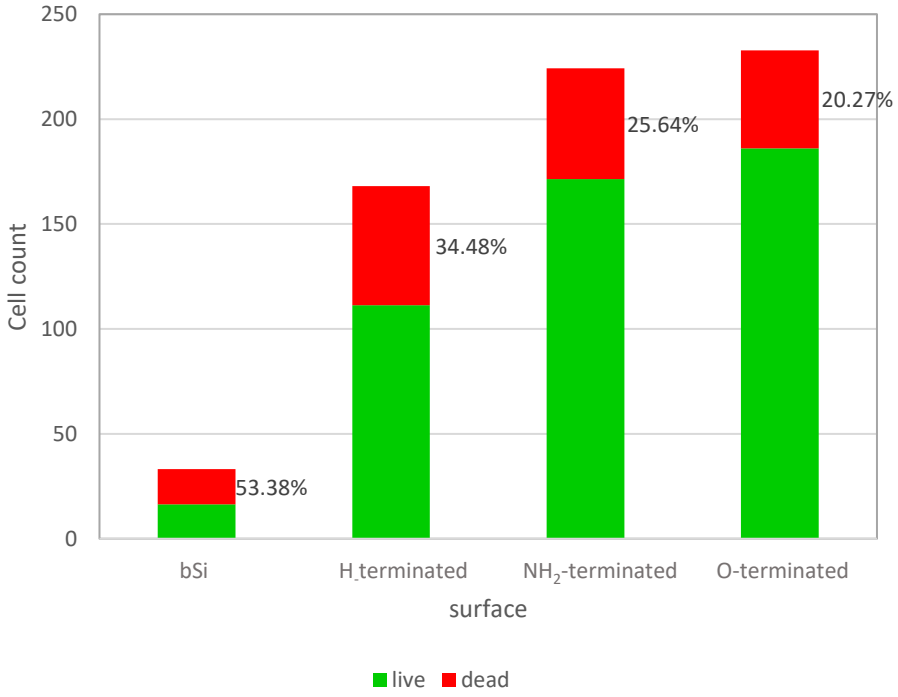

Figure 22 - Graph displaying effect of surface-termination of diamond films on cell density and death percentage, compared to bSi control.

Focusing on the impact on cell death percentage, increasing hydrophilicity resulted in a decrease in cell death ratio of almost 15% comparing H-terminated to O-terminated. However, looking at the actual values of dead cell counts there is little variation across the 3 D-bSi samples– the decrease in observed percentage is as a result of the increasing population of live cells. This shows that despite increased hydrophilic character causing increased attraction of bacteria to a surface, this does not correspond to an increase the number of cells that are able to be mechanically killed by the NSS, suggesting that the hydrophilicity causes the cells to adhere in a way that does not cause death – *i.e.* through interaction of the EPS and fimbriae with the hydrophilic groups, preventing direct contact of the cell membrane with the nanostructure.

3.5.6 Surface hydrophobicity

Shown in Figure 24, a decrease in hydrophilicity as achieved by F-termination of the D-bSi produced the expected results. By comparison to H-terminated, the F-terminated surface showed 1/3 the observed cell adhesion, indicating that bacteria experienced lower attractive and adhesive forces to the diamond. Total dead cell count was lower for F-terminated, but percentage of dead cells increased with hydrophobic character, suggesting that of the cells that were able to adhere, this was more frequently due to the physical interaction that results in cell death. If this process of adhesion was not able to take place, the cell is more easily repelled away from the surface, illustrated by the much lower live cell count.

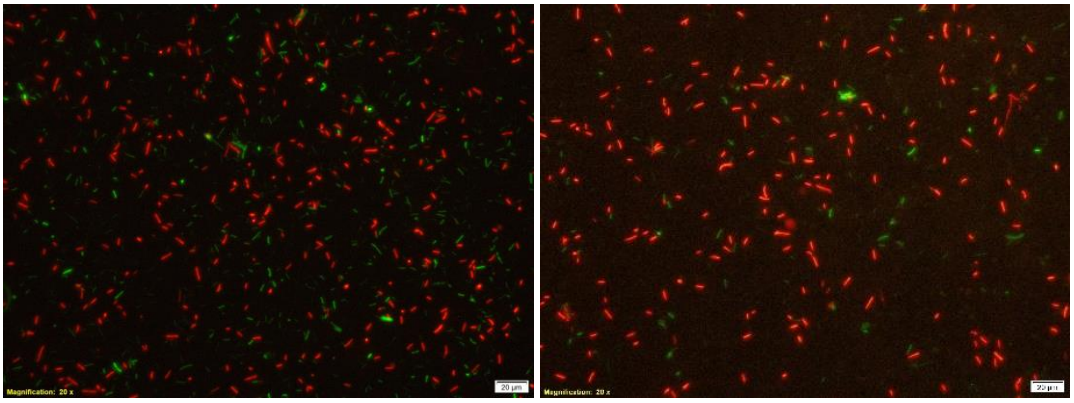

Figure 23 - Fluorescence micrographs showing effect of increased hydrophobicity on cell adhesion

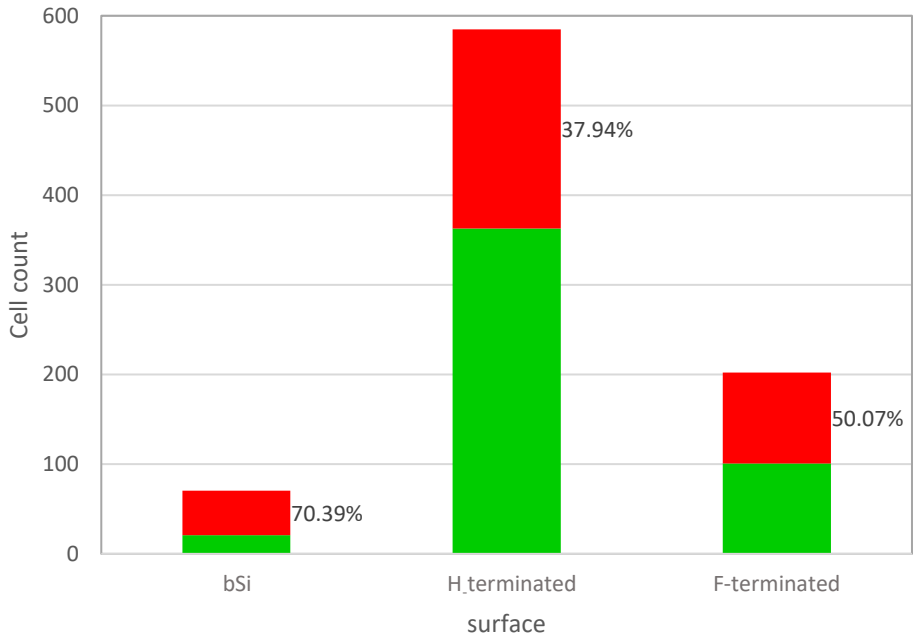

Figure 24 - Graph displaying the variation in cell adhesion and death with change in surface termination.

3.6 OBSERVATIONS

3.6.1 Visual evidence of killing mechanism

Surface-adhered bacteria were examined using SEM. By comparing the morphology of *E. coli* cells on a flat surface to a NSS, differences can be observed. Figure 27 illustrates that on both flat Si and diamond surfaces, the cells appear healthy – they are cylindrical in shape, have started to multiply and are expressing fimbriae. Comparatively, cells in contact with D-bSi shown in Figure 28 were shown to have undergone deformation, no-longer turgid and regular cylinders, stretched non-uniformly between points of contact.

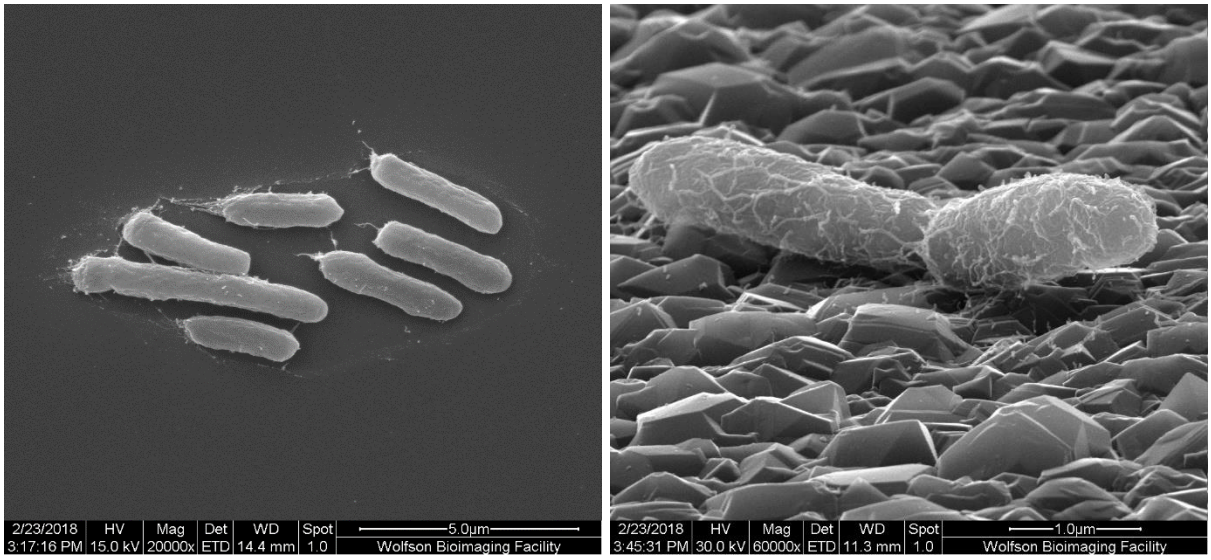

Figure 27 - Examples of healthy turgid bacteria cells on flat Si (left) and flat diamond (right) control surfaces

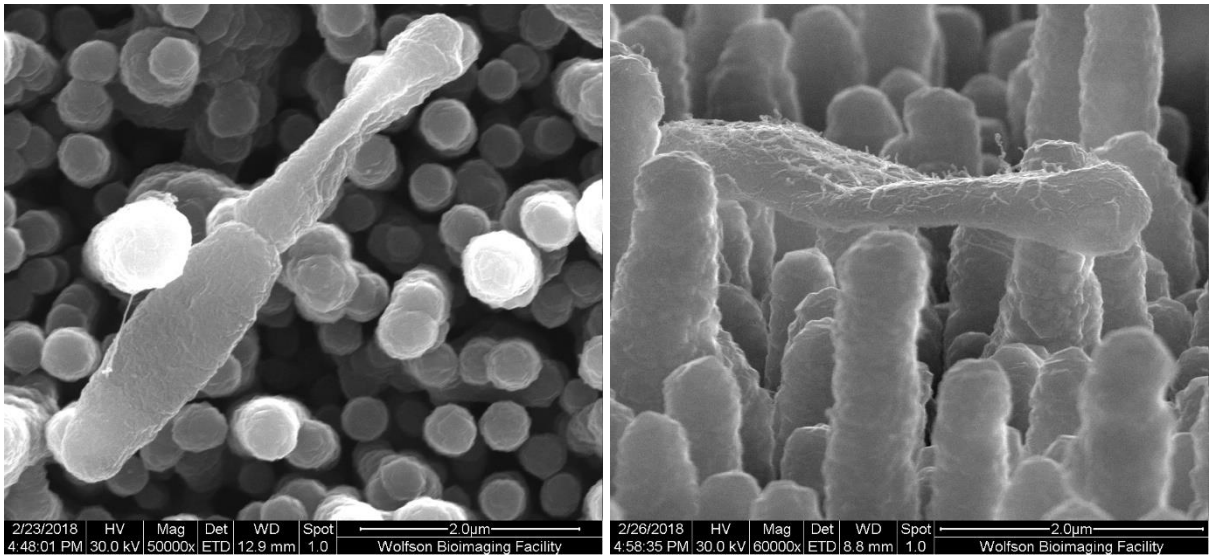

Figure 28 - SEM images of E. coli *cells adhered to D-bSi surfaces.*

Further evidence of this physical mechanism of cell death was revealed using fluorescence microscopy. Figure 25 shows cell population of a section of D-bSi surface that was manually scratched before cell cultivation, resulting in destruction of the needles producing a surface topography similar to that shown in Figure 13. The location of the needle scratch can be easily identified by the higher concentration of live cells and lower concentration of dead cells that are present along that strip.

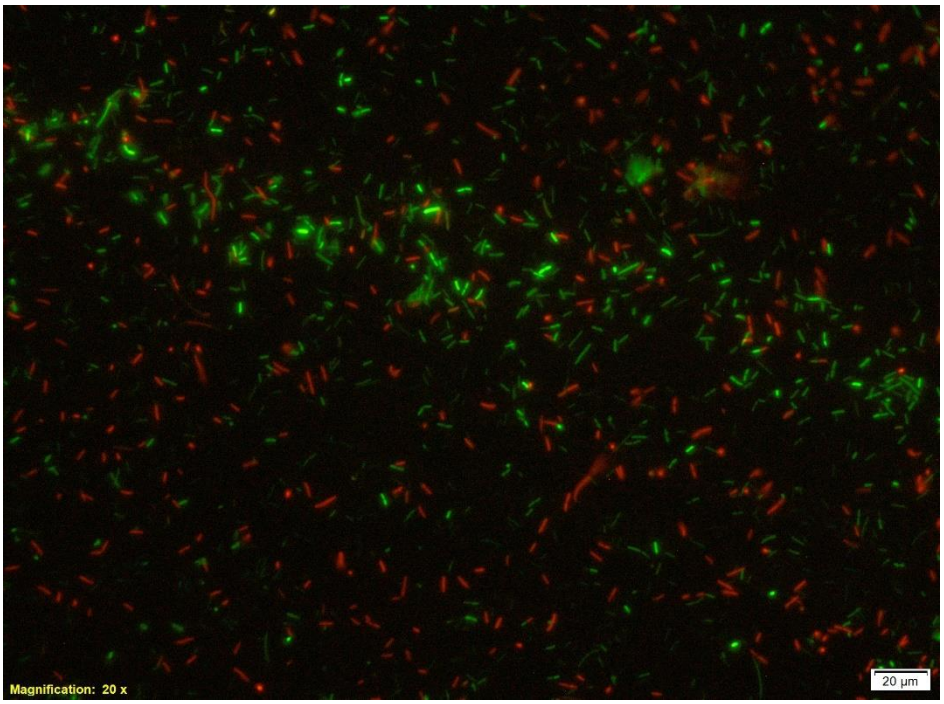

Figure 25 - Fluoresence microscopy image of D-bSi surface featuring a manual tweezer scratch.

3.6.2 Non-bactericidal cell adhesion

SEM imaging also revealed the occurrence of cellular adhesion to the nanostructured surfaces without onset of cell death. Cells were observed to rest on the tips of the bSi needles provided there were enough points of contact (Figure 26) without deformation of the cell occurring. Cell adhesion through anchoring of the cells to the spikes by the cellular fimbriae was also shown to occur **Error! Reference source not found.**. This effectively allows the cell to suspend itself from the spikes, preventing sinking of the cell onto the spikes from occurring and therefore cell death.

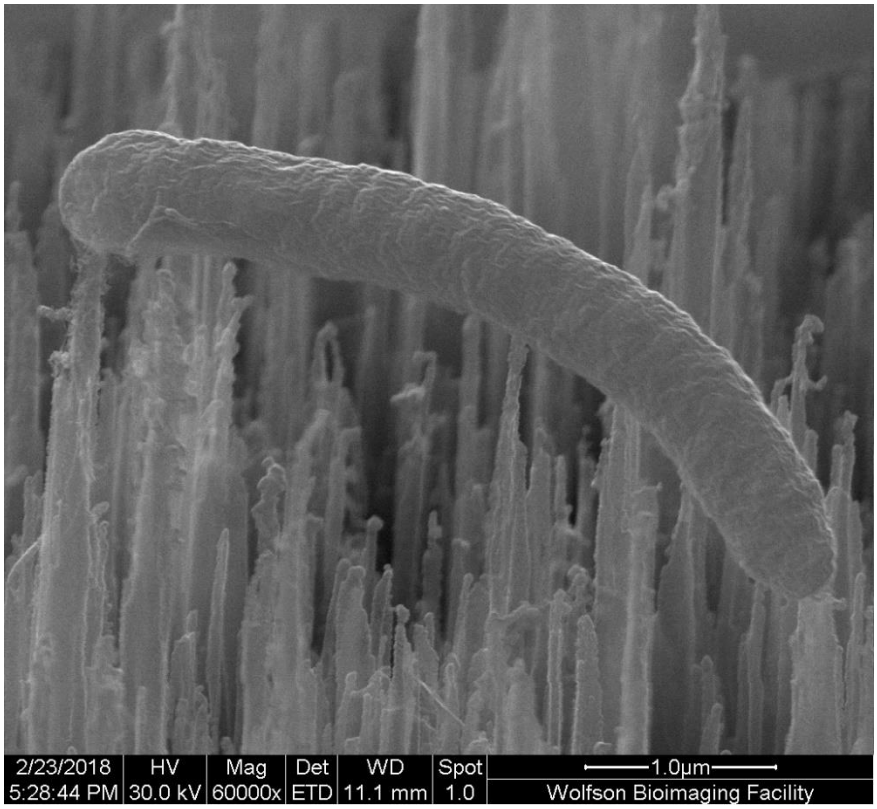

Figure 26 - Image showing healthy bacteria cell resting on bSi spikes

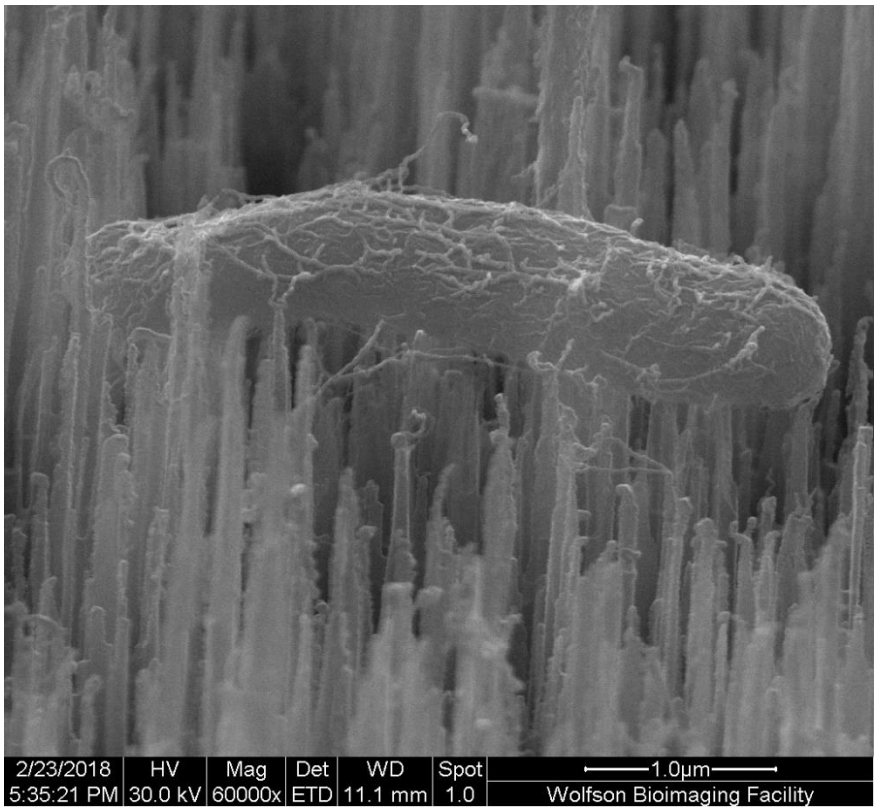

Figure 27 - Image of a bacterial cell suspended between bSi spikes by its fimbriae.

4 CONCLUSIONS

The knowledge of the bactericidal activity of bSi was expanded through testing of a sample with new dimensions to add to the database. The sample was shown to have the highest cell death percentage yet achieved by the group of almost 60%. It was theorised that this improvement could in part be attributed to the bimodal distribution of needle heights minimising the bed-of-nails effect and causing increased entrapment of cells, as a sample of comparable needle density but spikes of uniform length of 20 µm has shown less than half this cell death percentage.

Bactericidal activity was shown to be retained upon coating with a diamond film, although a reduction in cell death percentage was observed. This was caused by an increase in tip diameter of the needles resulting in less strain exerted on the cell membrane due to an increased contact surface area. Cell adhesion quadrupled when comparing uncoated to coated bSi, again influenced by larger surfaces areas for potential contact, as well as a reduction in surface roughness and increased wettability.

Visual evidence of cell deformation on contact with nanostructures served to further confirm the theorised physical mechanism of cell death.

Diamond coated black silicon needles that exhibited both hydrophobic and hydrophilic properties were able to be successfully produced through exposure to plasma, with intent to create different surface terminations. This was confirmed by changes in observed contact angles.

The effect of surface hydrophilicity on cellular adhesion was established, with the trend showing increasing surface wettability lead to increased cell proliferation. However, increased adhesion did not lead to increased cell death, further confirming that cell death occurs through a purely physical mechanism, and suggesting that increased attraction of cells to a surface can increase the occurrence of non-lethal adhesion interactions, such as the anchoring of cells by fimbriae.

In summary, cell death is governed entirely by physical properties of the surfaces, most notably dimensions of the nanopillar – it is unaffected by changes in surface wettability. Cell adhesion however is influenced by both physical and chemical interactions, non-specific and specific.

A basic test of mechanical durability was used to determine that diamond coating of bSi with a thickness of the order of 100s of nanometres does not provide any benefit to durability, with the nanostructures still easily crushed and broken.

Looking at the results from the approach of finding a material that combines bactericidal and bacteria-resistant properties, the best performance was conclusively the bSi, producing both highest death rate and lowest cell adhesion.

5 FUTURE WORK

5.1 SURFACE FABRICATION

There are countless different parameters that can be varied to investigate optimisation of these composite materials.

Continuation of this area of research should focus on further variation of dimensions of bSi needles to more clearly elucidate the effect each parameter has on cell death percentage. The combined parameter fraction of available surface area should continue to be used as a reference point, but when possible, needle density and tip diameter should also be varied in isolation, as these impart the biggest differences in performance.

Characterisation of optimisation of the surface terminated films, through methods such as XPS to determine concentration of the new groups on the surface of the film, followed by further experiments varying degree of surface termination would more thoroughly determine the trend observed with cell adhesion. Other surface functionalisation techniques and groups could also be investigated such as attachment of polymeric chains.

Moving forward with D-bSi as a viable new bactericidal material, a compromise between a diamond coating thick enough to impart any actual benefit to hardness, and thin enough that tip diameter remains small enough to retain bactericidal activity must be found. As such, a maximum diamond growth duration that exhibits these two benefits should be looked into. If not, there is not a realistic future for D-bSi in this area of research, as diamond coating has been shown to reduce bactericidal capabilities without imparting any benefit compared to uncoated bSi.

5.2 BACTERIAL TESTING

Regarding method of determining cell viability, a more repeatable and consistent method than Live/Dead assays would be preferred, potentially moving towards the use of metabolic studies to determine cell activity. Incubation time of bacteria on the surfaces should also be varied to establish if cell death has a dynamic component, - whether or not cells sink onto the surface and if this affects cell death.

6 REFERENCES

[1] R. M. Klevens, J. R. Edwards, C. L. Richards, T. C. Horan, R. P. Gaynes, D. A. Pollock, D. M. Cardo, *Public Health Rep.*, **2007,** 122, 160-166.

[2] S. A. Onaizi, S. S. J. Leong, *Biotech. Adv.*, **2011**, 29, 67–74.

[3] A. G. Gristina, *Science*, **1987**, 237, 1588–1595.

[4] R.M. Donlan, *Emerg. Infect Dis.*, **2002**, 8, 881-890.

[5] C.T. Huang, F.P. Yu, G.A. McFeters, P.S. Stewart, *Appl. Environ. Microbiol*., **1995**, 61(6), 2252-2256.

[6] S. B. Luppens, M. W. Reij, R. W. van der Heijden, F. M. Rombouts, T. Abee, *Appl. Environ. Microbiol*, **2002**, 68, 4194–4200.

[7] D. Davies, *Nat. Rev. Drug Disc.*, **2003**, 2, 114–122.

[8] L. Passerini, K. Lam, J. W. Costerton, E. G. King, *Crit. Care Med.*, **1992**, 20, 665–673.

[9] B. Pruess, *NDSU Agriculture Commun.* **2011,** (701) 231-784.

[10] S. Baker, C. Griffiths, J. Nicklin, *Microbiology*, Garland Science, 4th edn., **2011**, 46-56.

[11] T. J. Silhavy, D. Kahne, S. Walker, *Cold Spring Harb. Perspect. Biol.*, **2010**, 2:a000414.

[12] H. Connell, W. Agace, P. Klemm, M. Schembri, S. Marild, C. Svanborg, *Proc. Natl. Acad. Sci. USA*, **1996**, 93, 9827-9832.

[13] S. Rajabzadeh, R. Sano, T. Ishigami, Y. Kakihana, Y. Ohmukai, H. Matsuyama, *Appl. Surf. Sci.*, **2015**, 324, 718–724.

[14] M. Morra, C. Cassineli*, J. Biomater. Sci. Polym. Ed.,* **1999**, 10, 1107-1124.

[15] B. Wang, Z. Ye, Y. Tang, Y. Han, Q. Lin, H. Liu, H. Chen, K. Nan, *Int. J. Nanomedicine*, **2017**, 12, 111–125.

[16] A. Pierres, A. Benoiel, D. Touchard, P. Bongrand, *Biophys. J.,* **2008**, 94, 4114-4122.

[17] E. Ostuni, R. G. Chapman, R. E. Holmlin, S. Takayama, G. M. Whitesides, *Langmuir*, 2001, 17, 5605–5620.

[18] N. Maximous, G. Nakhla, W. Wan*, J. Membrane Sci.*, 2009, 339, 93-99.

[19] I. Banerjee, R. C. Pangule, R. S. Kane, *Adv. Mater.*, **2011**, 23(6), 690-718.

[20] F. Hizal, N. Rungraeng, J. Lee, S. Jun, H. J. Busscher, H. C. van der Mei, C. Choi, *ACS Appl. Mater. Interfaces*, **2017**, 9(13) 12118-12129.

[21] A. Marmur, *Biofouling*, **2006**, 22, 107-115.

[22] E. Biazar, M. Heidari, A. Asefnezhad, N. Montazer, *Int. J. Nanomedicine*, **2011**, 6, 631–639.

[23] R. N. Wenzel, *Ind. Eng. Chem*., **1936**, 28, 988–994.

[24] P. Decuzzi, M. Ferrari, *Biomater*., **2010**, 31, 173-179.

[25] J. C. Tiller, C. Liao, K. Lewis, A. M. Klibanov, *Proc. Natl. Acad. Sci. U.S.A.*, **2001**, 98, 5981-5985.

[26] A. D. Russell, *J. Antimicrob. Chemother*, **2004,** 53, 693–695.

[27] A. Tripathy, P. Sen, B. Su, W. H. Briscoe, *Adv. Colloid Interface Sci.*, **2017**, 248, 85-104.

[28] N. Li, P. Berton, C. Moraes, R. D. Rogers, N. Tufenkji, *Adv. Colloid Interface Sci.*, **2017**.

[29] E. P. Ivanova, J. Hasan, H.K. Webb, V. K. Truong, G.S. Watson, J.A. Watson, V.A. Baulin, Sergey Pogodin, J.Y. Wang, M.J. Tobin, C. Löbbe, R.J. Crawford, *Small*, **2012**, 16, 2489-2494.

[30] C. D. Bandara, S. Singh, I. O. Afara, T. Tesfamichael, A. Wolff, K. Ostrikov, A. Oloyede, *ACS Appl. Mater. Interfaces*, **2017,** 9, 6746–6760.

[31] X. Li, G. S. Cheung, G. S. Watson, J. A. Watson, S. Lin, L. Schwarzkopfe, D. W. Green, *Nanoscale*, **2016**, 8, 18860-18869.

[32] G. S. Watson, D. W. Green, L. Schwarzkopf, X. Li, B. W.Cribb, S. Myhr, J. A.Watson, *Acta. Biomater*., **2015**, 21, 109-122.

[33] S. Pogodin, J. Hasan, V. A. Baulin, H. K. Webb, V. K. Truong, T. H. Phong Nguyen, V. Boshkovikj, C. J. Fluke, G. S. Watson, J. A. Watson, R. J. Crawford, E. P. Ivanova, *Biophys. J.*, **2013**, 104(4), 835-840.

[34] F. Xue, J. Liu, l. Guo, I. Zhang, Q. Li, *J. Theor. Biol.*, **2015**, 385, 1-7.

[35] X. Li, *Phys. Chem. Chem. Phys.*, **2016**, 18, 1311-1316.

[36] H. Persson, Z. Li, J. O. Tegenfeldt, S. Oredsson, C. N. Prinz, *Scientific Reports*, **2015**, 5, 18535.

[37] T. Diu, N. Faruqui, T. Sjöström, B. Lamarre, H. F. Jenkinson, B. Su, M. G. Ryadnov, *Scientific Reports,* **2014**, 4, 7122.

[38] C. Sengstock, M. Lopian, Y. Motemani, A. Borgmann, C. Khare, P. J. Buenconsejo, T. A. Schildhauer, A. Ludwig, M. Köller, *Nanotechnology*, **2014**, 16, 25.

[39] S. Wu, F. Zuber, J. Brugger, K. Maniura-Weber,, Q. Ren, *Nanoscale*, **2016,** 8, 2620-2625.

[40] H. Jansen, M. de Boer, R. Legtenberg and M. Elwenspoek, *J. Micromech. Microeng.*, **1995,** 5, 115.

[41] E. P. Ivanova, J. Hasan, H. K. Webb, G. Gervinskas, S. Juodkazis, V.Khanh Truong, A. H.F. Wu, R. N. Lamb, V. A. Baulin, G. S. Watson, J. A. Watson, D. E. Mainwaring, R. J. Crawford, *Nature Commun.*, **2013**, 4, 2838.

[42] V. T. H. Pham, V. Khanh Truong, A. Orlowska, S. Ghanaati, M. Barbeck, P. Booms, A. J. Fulcher, C. M. Bhadra, R. Buividas, V. Baulin, C. J. Kirkpatrick, P. Doran, D. E. Mainwaring, S. Juodkazis, R. J. Crawford, E. P. Ivanova, *ACS Appl. Mater. Interfaces*, **2016**, 8, 22025–22031,

[43] W. G. Eversole, **1958** US Patent nos 3030187, 3030188.

[44] W. Banholzer, *Surf. Coat. Technol.*, **1992**, 53, 1-12.

[45] H. Kawarada, *Surf. Sci. Rep.* **1996**, 26, 205-259.

[46] P. W. May, *Phil. Trans. R. Soc. Lond. A*, **2000,** 358, 473-495.

[47] M.C. Salvadori, W.W.R. Araújo, F.S. Teixeira, M. Cattani, A. Pasquarelli, E.M. Oks, I.G. Brown, *Diamond & Relat. Mater.*, **2010**, 19, 324–328.

[48] S. Kuga, J.-H. Yang, H. Takahashi, K. Hirama, T. Iwasaki, H. Kawarada, *J. Am. Chem. Soc.*, 2008, 130, 13251-13263.

[49] D. Zhu, J. A. Bandy, S. Li, R. J. Hamers, *Surf. Sci.*, **2016**, 650, 295–301.

[50] Y. Liu, V. N. Khabashesku, N. J. Halas, *J. Am. Chem. Soc.*, 2005, *127*, 3712–3713.

[51] S. Ferro, A. De Battisti, *J. Phys. Chem. B*, 2003, 107, 7567–7573.

[52] M.A. Ray, T. Tyler, B. Hook, A. Martin, G. Cunningham, O. Shenderova, J.L. Davidson, M. Howell, W.P. Kang, G. McGuire, *Diamond Relat. Mater.*, **2007**, 16, 2087.

[53] K.F. Chong, PhD thesis, National University of Singapore, **2009**, available from scholarbank.nus.edu.sg/handle/10635/17738

[54] P. W. May, M. Clegg, T. A. Silva, H. Zanin, O. Fatibello-Filho, V. Celorrio, D. J. Fermin, C. C. Welch, G. Hazell, L. Fisher, A. Nobbse and B. Su, *J. Mater. Chem. B*, **2016**, 4, 5737-5746.

[55] P. Taylor, MSci Dissertation, University of Bristol, **2017**.

[56] S.A. Rakha, C. Jianqing, X. Huihao, y. Guojun, D. Zhu, J. Gong, *Diamond Relat. Mater.*, **2009**, 18, 1247–1252.

[57] S. Prawer, R. J. Nemanich, *Phil. Trans. R. Soc. Lond. A*, **2004**, 362, 2537–2565.

[58] A. C. Ferrari, J. Robertson, *Phys. Rev. B*, **2001**, 63, 121405.